ACS OMEGA

http://pubs.acs.org/journal/acsodf

Article

Geochemical Changes in the Late Ordovician to Early Silurian Interval in the Northern Margin of the Upper Yangtze Platform, Southern China: Implications for Hydrothermal Influences and Paleocean Redox Circumstances

Xiang Fu, Xuan Liu,* Shuzhen Xiong, Xu Li, Qixuan Wu, and Bin Xiao

Cite This: *ACS Omega* 2023, 8, 13078−13096

Read Online

ACCESS | Metrics & More | Article Recommendations

ABSTRACT: A comprehensive chemostratigraphic study, including evaluation of rare earth elements and trace elements, was conducted to explain the paleoenvironments of the northern margin of the Upper Yangtze Platform. Trace elements, like Ba, U, V, Cu, and Zn, tended to be more abundant in these formations than in the upper continental crust. The authigenic abundances of Al-normalized U and V, as well as the Th/U and V/Sc ratios, were used as indicators of the redox circumstances. In the Nanjiang area, the redox circumstances of the bottom water during the Ordovician−Silurian transition changed from oxic in the Late Katian to slightly anoxic in the Hirnantian and then gradually became anoxic in the Early Rhuddanian. In the Chengkou area, the redox circumstances of the bottom water during the Ordovician−Silurian transition abruptly changed from oxic in the Late Katian to strongly anoxic in the Hirnantian and continued to become more anoxic until the Rhuddanian. The total organic carbon concentrations were well correlated with the redox circumstances of the bottom water. We conclude that the transient hydrothermal activity was not widely distributed during the Late Ordovician−Early Silurian transition, and it might also have been only a local event in the Upper Yangtze Platform. The enrichment in organic matter was mostly sourced from the photic zone and was governed by the redox circumstances of the bottom water.

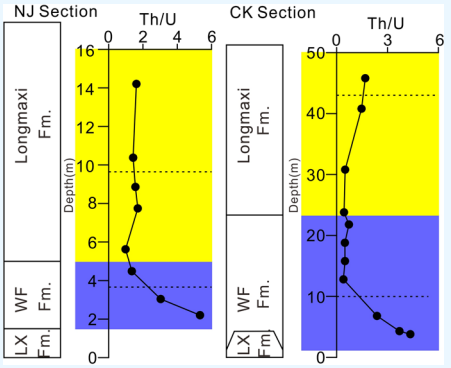

1. INTRODUCTION

The Ordovician−Silurian transition was a critial epoch in Earth's history and was distinguished by large-scale glaciation, marine mass extinction, extensive volcanism, and sea level and global environmental changes.[1−5] During this transitional period, organic-rich marine shales and mudstones built up in a variety of paleogeographic environments, from the deep shelf to the base of the continental slope.[6−8] Several of these shales and mudstones are considered significant petroleum source rocks.[4,9−12] Many geobiology, geochemistry, and petrology studies have been done on these successions due to the debates surrounding the triggering mechanisms of these contemporaneous processes and the enrichment of organic materials. However, most previous research studies have reported geochemical data for the southern part of the Upper Yangtze Platform, and data for the northern part of the platform have rarely been reported.[1,4,13−15] The main reason for this is that the northern margin of the Upper Yangtze Platform is not a favorable zone for conventional oil and gas exploration due to its complex tectonic deformation, so little oil and gas exploration work has been conducted in this area, which limits the study of the Late Ordovician and Early Silurian geological and geochemical characteristics in this area.

Unconventional gas exploration and development has ramped up in recent years to keep up with rising demand for domestic natural gas output. The Sichuan Basin is one of the largest oil and gas basins in China, and it is home to a wealth of natural gas resources, as well as a number of notable accomplishments in the fields of unconventional gas exploration and development.[16,17] In the Sichuan Basin and neighboring formations, shale gas fields such as the Fuling, Weirong, Weiyuan, Changning, and Zhaotong plays were identified between 2012 and 2020.[18,19] More and more geological information has been gathered, as shale gas drilling has progressed in the eastern parts of Chongqing and southern Sichuan. Therefore, we have a thorough comprehension of the geochemical features and

Received: January 17, 2023
Accepted: March 14, 2023
Published: March 28, 2023

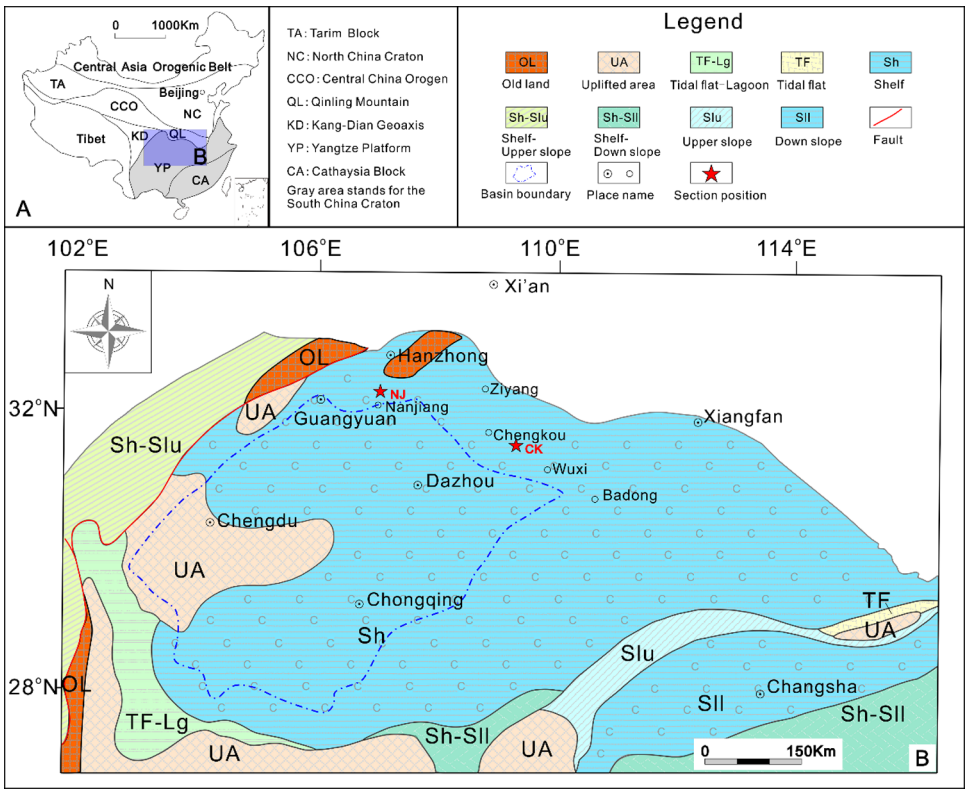

Figure 1. Simplified geological map of the Upper Yangtze Platform and its neighboring area. (A) Location of the study area and (B) basic geologic setting of the study area (modified after Huang et al.[24]).

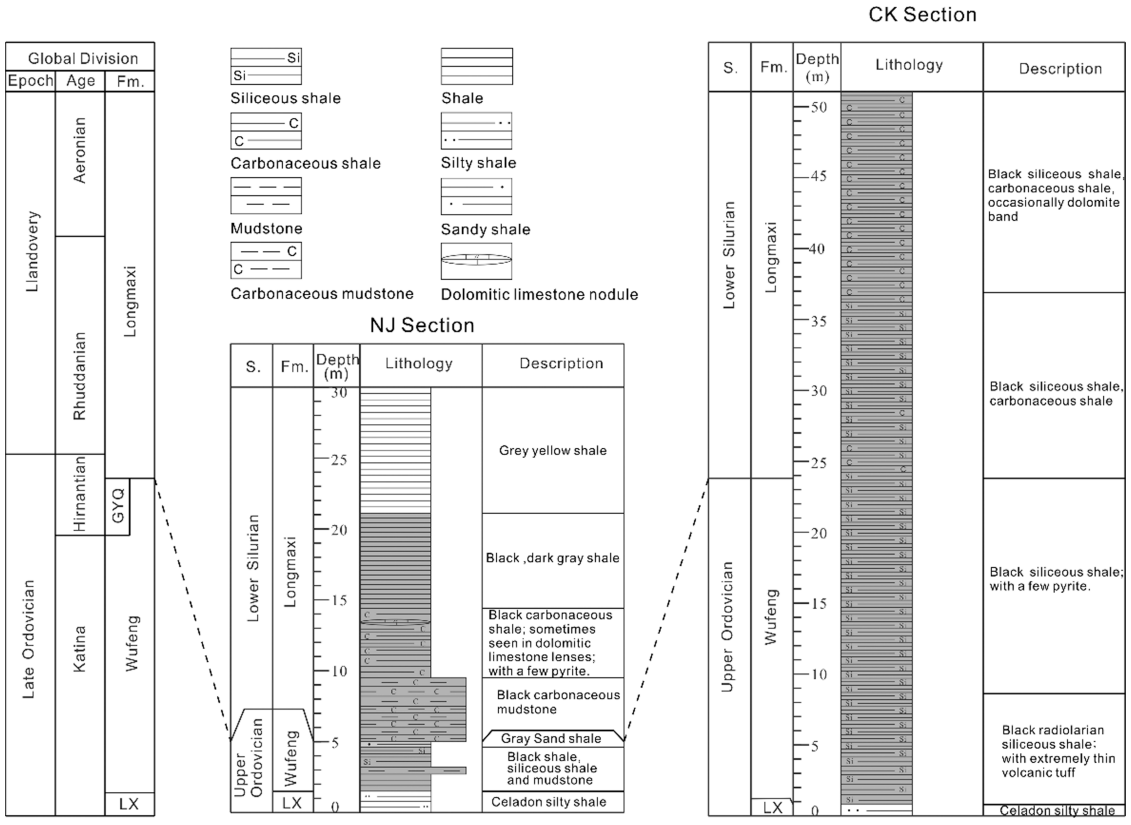

Figure 2. Lithologic profile of the NJ section in Sichuan Province and the CK section in the Chongqing Municipality, southern China.

sedimentary setting of the Late Ordovician Wufeng Formation (WF) and the Early Silurian Longmaxi Formation (LMX) in these regions. Using drilling cores from a shale gas demonstration location, Chen et al. described the evolution of

https://doi.org/10.1021/acsomega.3c00277
ACS Omega 2023, 8, 13078−13096

Table 1. Major Element Contents (in wt % Oxide) for Samples from the NJ Section in Sichuan Province and the CK Section in the Chongqing Municipality, Southern China

formation	samples	depth (m)	SiO_2	TiO_2	Al_2O_3	MnO	MgO	CaO	Na_2O	K_2O	P_2O_5	TFe_2O_3	LOI	total
NJ section														
Wufeng	NJ01-2D	2.20	63.02	0.85	16.59	0.073	2.26	0.298	0.794	4.40	0.08	6.43	4.85	99.65
	NJ01-3D	3.04	69.86	0.73	13.50	0.004	1.23	0.109	0.313	4.07	0.09	4.67	5.09	99.66
	NJ01-4D	4.49	78.29	0.43	9.23	0.004	0.763	0.139	0.341	2.46	0.35	1.32	6.36	99.69
Longmaxi	NJ01-5D	5.62	74.16	0.80	12.33	0.007	0.958	0.148	0.693	3.41	0.05	1.08	6.04	99.67
	NJ01-6D	7.75	72.27	0.69	13.01	0.004	0.995	0.058	0.456	3.49	0.05	1.24	7.46	99.72
	NJ01-7D	8.86	78.70	0.50	9.20	0.006	0.677	0.058	0.474	2.37	0.05	1.24	6.41	99.69
	NJ01-8D	10.38	72.77	0.57	10.51	0.008	0.867	0.084	0.714	2.93	0.06	4.31	6.88	99.70
	NJ01-11D	14.21	71.32	0.69	13.69	0.008	1.04	0.071	0.962	3.78	0.07	1.80	6.24	99.67
CK section														
Wufeng	CK03-6D	3.80	87.67	0.20	4.25	0.09	0.78	0.89	0.3	1.03	0.05	2.24	2.52	100.02
	CK03-7D	4.30	77.58	0.27	5.89	0.05	0.85	0.68	0.3	1.53	0.05	6.80	6.31	100.31
	CK03-9D	6.80	89.43	0.16	3.25	0.03	0.46	0.31	0.26	0.75	0.04	1.53	3.08	99.30
	CK03-13D	12.80	83.58	0.32	5.23	0.02	0.45	0.21	0.5	1.37	0.08	1.85	6.81	100.42
	CK03-14D	15.80	79.65	0.39	6.67	0.01	0.53	0.22	0.65	1.77	0.10	2.46	7.97	100.42
	CK03-15D	18.80	79.57	0.44	6.79	0.02	0.55	0.25	0.7	1.81	0.11	3.03	7.23	100.50
	CK03-16D	21.80	79.85	0.46	7.11	0.01	0.57	0.27	0.63	1.95	0.12	2.55	7.02	100.54
Longmaxi	CK03-17D	23.80	79.42	0.55	5.66	0.01	0.70	1.11	0.56	1.46	0.10	2.35	7.14	99.06
	CK03-18D	30.80	78.70	0.44	6.46	0.06	0.52	0.29	0.67	1.73	0.11	3.66	7.27	99.91
	CK03-22D	40.80	65.64	0.68	14.33	0.06	2.17	0.75	1.02	3.36	0.12	5.67	6.25	100.05
	CK03-25D	45.80	70.74	0.59	12.73	0.04	1.86	0.47	0.96	2.94	0.10	4.79	5.17	100.39

the graptolite zones and classified the WF into four graptolite zones (WF1−WF4) and the LMX into nine graptolite zones (LM1−LM9).[20] The Chengkou-Wuxi area is where most of the drilling for shale gas in the WF-LMX on the northern edge of the Upper Yangtze Platform has been done. In previous studies, the stratigraphic and lithologic features and gas-bearing properties of these wells were looked at in detail.[21−23] However, there has not been a lot of studies done on the geochemical shifts that have taken place on the northern edge of the Upper Yangtze Platform and how those shifts have affected the richness of organic matter.

In this study, we conducted a comprehensive chemostratigraphic study, including evaluation of major, trace, and rare earth elements (REEs), of the Late Ordovician and Early Silurian siliceous shale succession in the northern margin of the Upper Yangtze Platform (Figure 1) to illustrate how significant environmental and oceanic changes affect organic matter accumulation.

2. GEOLOGIC SETTINGS

To the north lies the Yangtze Platform, and to the south are the Cathaysia continental blocks, which together make up southern China. (Figure 1A).[24−26] As a consequence of the merging of the Yangtze and Cathaysia blocks in the southeast during the Late Ordovician−Early Silurian transition, the Yangtze shallow water carbonate platform eventually transformed into a siliciclastic-dominated deep shelf basin.[24] The Upper Yangtze Platform was encircled by Cathaysian Land, the Dianqian Uplift, and the Chengdu Uplift, which together formed a semi-enclosed bay that expanded toward the north during the Late Ordovician.[24,25] Two field sections, located in Nanjiang County, Sichuan Province, and Chengkou County, Chongqing Municipality, 200 km apart, were selected for the geochemical study. Paleographically, the Nanjiang section (NJ section) was deposited on the shallower inner shelf, adjacent to the northern Hanzhong uplift, whereas the Chengkou section (CK section) was deposited on the deeper outer shelf (Figure 1B).

The Ordovician−Silurian border layers consist of both the WF (Fm.) and the LMX (Figure 2). Their ages are well restricted by graptolites biostratigraphic data.[27,28] Following one other in increasing sequence, the Linxiang formation, WF, and LMX make up the Late Ordovian-Early Silurian strata revealed in the NJ and CK sections (Figure 2). Regarding the NJ section, data gathered from the field suggest that the Linxiang celadon silty shale is overlain by the Wufeng black shale, mudstone, and sandy shale, which is overlain by the Longmaxi black carbonaceous mudstone and shale (Figure 2). Regarding the CK section, data gathered from the field suggest that the Linxiang celadon silty shale is overlain by the Wufeng black radiolarian siliceous shale with extremely thin volcanic tuff and a minor amount of pyrite. These deposits are overlain by the LMX black siliceous and carbonaceous shale, which contain thin siliceous dolomite beds (Figure 2).

3. MATERIALS AND METHODS

In this study, 8 samples from the NJ section and 11 samples from the CK section were taken from the northern boundary of the Upper Yangtze Platform. These samples were mainly from the Late Ordovician WF and the Early Silurian LMX. Detailed sample information and test results are presented in Tables 1−4. Eleven samples were subjected to major element analysis, and some of the trace element data for the CK section are from the literature.[25]

Nineteen geochemical samples were analyzed. The major element analysis of fused glass composed from a mixture of sample powder and flux with a 1:5 ratio was conducted using the automatic X-ray fluorescence spectrometer (XRF-1500) at the Institute of Geology, Chinese Academy of Geological Sciences. The Institute of Tibetan Plateau Research, Chinese Academy of Sciences, used the VG PQ2 Turbo inductively coupled plasma source mass spectrometer to dissolve the samples and analyze it for trace elements. First, 0.500 mL (1 + 1) of HNO_3 and 1.00 mL of HF were used to digest 25.0 mg of rock powder (200 mesh) in a firmly closed Teflon screw-cap beaker. The dried sample was

https://doi.org/10.1021/acsomega.3c00277
ACS Omega 2023, 8, 13078−13096

Table 2. Trace Element Contents (ppm) and Relative Ratios for the Samples from the NJ Section in Sichuan Province and the CK Section in the Chongqing Municipality, Southern China

samples	depth (m)	Li	Sc	Ti	V	Cr	Co	Ni	Cu	Zn	Rb	Sr	Zr	Nb	Cs	Ba	Hf	Ta	Tl	Pb	Th	U
NJ section																						
Wufeng Formation																						
NJ01-2D	2.20	55.49	19.21	4850	117.5	76.29	28.53	150.8	93.07	316.7	202.4	46.38	151.2	22.51	11.54	1742	4.18	1.54	1.08	114.5	22.95	4.31
NJ01-3D	3.04	31.46	15.51	3981	161.9	258.3	4.06	163.0	103.6	40.90	183.6	53.26	148.6	18.81	10.56	2536	3.69	1.24	1.19	76.78	19.10	6.30
NJ01-4D	4.49	17.63	9.84	2385	354.2	67.06	1.10	32.21	87.70	16.40	104.0	82.63	89.48	14.29	5.75	1106	2.52	0.89	0.82	28.08	11.78	8.71
Longmaxi Formation																						
NJ01-5D	5.62	21.37	10.26	4368	252.3	64.18	1.00	13.69	28.69	24.95	157.9	43.17	299.2	72.29	8.22	2561	4.68	1.26	2.00	26.41	14.67	14.89
NJ01-6D	7.75	21.21	10.07	3756	222.2	52.31	0.85	15.47	7.50	11.94	155.7	44.61	322.8	35.04	9.68	2215	8.15	2.70	2.21	23.88	16.63	9.80
NJ01-7D	8.86	18.84	7.85	2804	175.6	46.66	1.45	20.79	14.18	10.35	109.8	50.84	161.0	22.42	6.73	1378	3.97	1.19	1.45	22.43	10.55	6.76
NJ01-8D	10.38	20.30	9.60	3094	226.1	53.90	4.44	37.41	10.57	221.7	138.3	33.94	131.2	14.57	8.21	1862	3.44	0.96	1.70	22.82	10.08	7.06
NJ01-11D	14.21	16.93	11.82	3397	164.8	61.64	1.96	15.82	12.80	28.32	159.5	39.24	150.8	16.09	9.95	1931	4.10	1.02	1.94	32.61	12.68	7.84
CK section																						
Wufeng formation																						
CK03-6D	3.80	43.99	5.08	1102	52.44	28.58	7.90	25.35	58.78	54.25	41.33	46.38	34.07	4.46	1.97	1301	0.96	0.31	0.21	15.82	4.97	1.14
CK03-7D	4.30	35.76	6.35	1518	124.7	54.17	11.97	56.67	100.1	115.7	61.28	41.09	58.90	6.84	3.13	1119	1.37	0.45	0.52	50.43	7.11	1.92
CK03-9D	6.80	46.25	3.32	876	105.0	41.81	3.44	27.18	62.57	119.8	31.69	31.05	31.59	3.62	1.63	1358	0.80	0.24	0.17	11.67	3.94	1.66
CK03-13D	12.80	18.14	5.12	1548	491.7	49.71	7.40	97.31	56.18	138.7	64.34	95.97	54.63	6.47	3.14	3440	1.42	0.43	0.63	12.86	6.32	15.85
CK03-14D	15.80	16.56	6.27	2002	524.2	54.81	5.61	87.90	62.96	100.6	79.83	83.68	73.51	8.43	4.18	2842	1.92	0.58	0.85	17.07	8.25	16.82
CK03-15D	18.80	16.07	6.39	2201	405.5	53.11	6.59	95.65	61.84	125.6	83.63	81.29	81.94	9.28	4.30	4350	2.15	0.63	1.66	17.00	8.89	18.34
CK03-16D	21.80	17.67	6.42	2405	332.8	53.16	6.21	88.27	49.85	109.6	91.52	85.08	118.6	16.67	4.71	4035	2.77	0.75	1.98	18.07	10.07	13.93
Longmaxi formation																						
CK03-17D	23.80	14.35	5.21	1725	263.4	38.14	7.24	110.9	45.82	126.6	67.25	97.08	76.45	10.49	3.36	12,530	1.92	0.54	1.75	12.41	7.19	16.60
CK03-18D	30.80	15.70	5.98	2072	403.0	49.78	10.54	110.3	60.66	165.3	79.80	89.84	78.84	8.75	4.07	5075	2.09	0.58	1.99	18.16	8.26	16.53
CK03-22D	40.80	44.91	14.32	3852	399.0	84.02	15.79	85.40	53.91	190.6	164.0	107.7	154.2	16.47	9.91	2602	4.07	1.14	2.67	24.94	13.41	9.14
CK03-25D	45.80	46.52	12.37	3453	257.8	74.29	13.72	72.88	52.54	174.9	142.1	83.04	171.3	25.99	8.48	1630	3.94	1.06	2.12	23.58	12.45	7.38

https://doi.org/10.1021/acsomega.3c00277
ACS Omega 2023, 8, 13078−13096

Table 3. Rare Element Contents (ppm) and Relative Ratios for the Samples from the NJ Section in Sichuan Province and the CK Section in the Chongqing Municipality, Southern China

samples	depth (m)	La	Ce	Pr	Nd	Sm	Eu	Gd	Tb	Dy	Y	Ho	Er	Tm	Yb	Lu	LREE	HREE	REE	LREE/HREE	Y/Ho
NJ section																					
Wufeng Formation																					
NJ01-2D	2.20	68.24	168.8	17.17	68.9	14.63	2.621	13.3	1.835	9.873	50.74	1.806	4.917	0.679	4.497	0.66	340.36	37.57	377.93	9.06	28.10
NJ01-3D	3.04	70.28	174.1	16.03	60.62	11.01	1.847	8.137	1.161	6.541	34.05	1.26	3.576	0.503	3.337	0.47	333.89	24.99	358.87	13.36	27.02
NJ01-4D	4.49	28.08	62.98	6.993	29.6	6.986	1.35	5.948	0.903	4.774	22.41	0.842	2.289	0.322	2.23	0.33	135.99	17.64	153.63	7.71	26.62
Longmaxi Formation																					
NJ01-5D	5.62	83.23	138	14.05	46.45	6.78	0.992	4.698	0.763	4.759	26.92	1.057	3.758	0.674	5.33	0.853	289.50	21.89	311.39	13.22	25.47
NJ01-6D	7.75	56.56	109.6	12.62	45.45	7.524	1.001	5.64	0.963	6.271	38.65	1.297	3.928	0.579	3.845	0.544	232.76	23.07	255.82	10.09	29.80
NJ01-7D	8.86	34.69	66.75	7.985	30.89	5.384	0.786	3.791	0.545	3.25	18.87	0.659	2.006	0.296	2.018	0.299	146.49	12.86	159.35	11.39	28.63
NJ01-8D	10.38	36.13	65.72	7.553	26.79	4.509	0.797	3.875	0.597	3.552	21.48	0.716	2.154	0.313	2.153	0.314	141.50	13.67	155.17	10.35	30.00
NJ01-11D	14.21	38.04	69.5	7.725	26.57	3.828	0.709	2.67	0.453	2.959	18.91	0.627	1.954	0.3	2.102	0.304	146.37	11.37	157.74	12.87	30.16
CK section																					
Wufeng Formation																					
CK03-6D	3.80	15.65	32.16	3.808	15.02	3.151	0.622	3.143	0.453	2.59	13.97	0.504	1.39	0.188	1.239	0.183	70.41	9.69	80.10	7.27	27.72
CK03-7D	4.30	24.27	43.94	5.842	23.1	4.906	0.978	5.005	0.735	4.277	24.47	0.849	2.417	0.345	2.211	0.33	103.04	16.17	119.21	6.37	28.82
CK03-9D	6.80	15.75	22.47	3.445	12.85	2.381	0.44	2.115	0.286	1.674	10.07	0.347	0.983	0.148	1.015	0.147	57.34	6.72	64.05	8.54	29.02
CK03-13D	12.80	21	37.12	5.124	20.48	3.97	0.818	4.29	0.634	3.799	28.57	0.774	2.195	0.306	1.879	0.272	88.51	14.15	102.66	6.26	36.91
CK03-14D	15.80	26.09	47.11	5.985	22.76	4.082	0.847	4.156	0.637	3.838	27.8	0.806	2.27	0.325	2.126	0.312	106.87	14.47	121.34	7.39	34.49
CK03-15D	18.80	26.46	48.39	5.826	22.26	4.175	0.837	3.878	0.598	3.496	21.77	0.701	2.012	0.29	1.878	0.27	107.95	13.12	121.07	8.23	31.06
CK03-16D	21.80	30.83	57.81	6.978	26.42	4.859	0.934	4.551	0.684	4.117	25.49	0.836	2.437	0.348	2.292	0.334	127.83	15.60	143.43	8.19	30.49
Longmaxi Formation																					
CK03-17D	23.80	21.74	40.88	5.158	20.34	4.091	0.904	4.23	0.578	3.367	21.14	0.673	1.913	0.271	1.744	0.256	93.11	13.03	106.15	7.14	31.41
CK03-18D	30.80	25.12	46.96	5.942	23.18	4.577	0.94	4.498	0.668	3.929	24.78	0.789	2.195	0.313	1.943	0.289	106.72	14.62	121.34	7.30	31.41
CK03-22D	40.80	39.65	73	9.13	34	6.374	1.311	5.776	0.857	5.058	30.26	1.018	2.933	0.428	2.79	0.407	163.47	19.27	182.73	8.48	29.72
CK03-25D	45.80	42.27	74.87	9.128	33.65	6.04	1.076	5.01	0.741	4.384	24.29	0.869	2.522	0.383	2.519	0.37	167.03	16.80	183.83	9.94	27.95

https://doi.org/10.1021/acsomega.3c00277
ACS Omega 2023, 8, 13078−13096

Table 4. Chosen Geochemical Indicators for Samples from the NJ Section in Sichuan Province and the CK Section in the Chongqing Municipality, Southern China

formation	samples	depth (m)	Eu/Eu*	Ce/Ce*	Y/Y*	Pr/Pr*	La_N/Yb_N	La_N/Ce_N	Dy_N/Sm_N	Th/U	V/Sc	V/Al	Cr/Al	Co/Al	Ni/Al	Cu/Al	Zn/Al	U/Al	Ba/Al	TOC (%)
NJ section																				
Wufeng	NJ01-2D	2.20	0.95	1.14	0.96	0.93	1.12	0.84	0.80	5.32	6.12	13.38	8.69	3.25	17.17	10.60	36.06	0.49	198.34	0.28
	NJ01-3D	3.04	0.94	1.20	0.95	0.91	1.55	0.84	0.70	3.03	10.44	22.65	36.14	0.57	22.81	14.50	5.72	0.88	354.83	0.64
	NJ01-4D	4.49	1.02	1.04	0.89	0.94	0.93	0.93	0.81	1.35	36.01	72.49	13.72	0.23	6.59	17.95	3.36	1.78	226.34	2.87
Longmaxi	NJ01-5D	5.62	0.80	0.93	0.96	1.02	1.15	1.26	0.83	0.99	24.59	38.65	9.83	0.15	2.10	4.40	3.82	2.28	392.33	2.43
	NJ01-6D	7.75	0.70	0.95	1.08	1.04	1.09	1.08	0.99	1.70	22.07	32.26	7.59	0.12	2.25	1.09	1.73	1.42	321.59	3.51
	NJ01-7D	8.86	0.83	0.93	1.03	1.02	1.27	1.08	0.72	1.56	22.38	36.05	9.58	0.30	4.27	2.91	2.13	1.39	282.92	3.26
	NJ01-8D	10.38	0.92	0.92	1.07	1.05	1.24	1.15	0.93	1.43	23.55	40.64	9.69	0.80	6.72	1.90	39.84	1.27	334.64	3.46
	NJ01-11D	14.21	1.00	0.94	1.11	1.04	1.34	1.14	0.92	1.62	13.94	22.74	8.50	0.27	2.18	1.77	3.91	1.08	266.43	2.58
CK section																				
Wufeng	CK03-6D	3.80	1.00	0.96	0.98	1.01	0.93	1.01	0.97	4.34	10.32	23.31	12.70	3.51	11.27	26.12	24.11	0.51	578.22	0.42
	CK03-7D	4.30	1.00	0.85	1.02	1.07	0.81	1.15	1.03	3.70	19.64	39.99	17.37	3.84	18.17	32.10	37.10	0.62	358.86	0.53
	CK03-9D	6.80	1.00	0.70	1.05	1.18	1.15	1.46	0.83	2.38	31.62	61.03	24.30	2.00	15.80	36.37	69.63	0.96	789.26	1.36
	CK03-13D	12.80	1.01	0.83	1.33	1.08	0.83	1.18	1.13	0.40	95.98	177.6	17.96	2.67	35.15	20.29	50.10	5.73	1242.6	3.58
	CK03-14D	15.80	1.03	0.87	1.26	1.06	0.91	1.15	1.12	0.49	83.64	148.4	15.52	1.59	24.89	17.82	28.48	4.76	804.59	3.22
	CK03-15D	18.80	1.02	0.90	1.11	1.03	1.04	1.14	0.99	0.48	63.43	112.8	14.77	1.83	26.61	17.20	34.94	5.10	1210.1	3.64
	CK03-16D	21.80	0.98	0.91	1.10	1.04	0.99	1.11	1.00	0.72	51.88	88.41	14.12	1.65	23.45	13.24	29.12	3.70	1072.0	4.05
Longmaxi	CK03-17D	23.80	1.13	0.89	1.12	1.04	0.92	1.11	0.98	0.43	50.54	87.90	12.73	2.42	37.01	15.29	42.25	5.54	4181.6	3.13
	CK03-18D	30.80	1.04	0.89	1.12	1.05	0.95	1.11	1.02	0.50	67.40	117.9	14.56	3.08	32.27	17.75	48.36	4.84	1484.8	4.56
	CK03-22D	40.80	1.07	0.89	1.06	1.07	1.05	1.13	0.94	1.47	27.86	52.59	11.07	2.08	11.26	7.11	25.12	1.21	342.98	1.93
	CK03-25D	45.80	0.95	0.88	0.99	1.06	1.24	1.18	0.86	1.69	20.84	38.25	11.02	2.04	10.81	7.80	25.95	1.10	241.86	1.76

https://doi.org/10.1021/acsomega.3c00277
ACS Omega 2023, 8, 13078−13096

http://pubs.acs.org/journal/acsodf

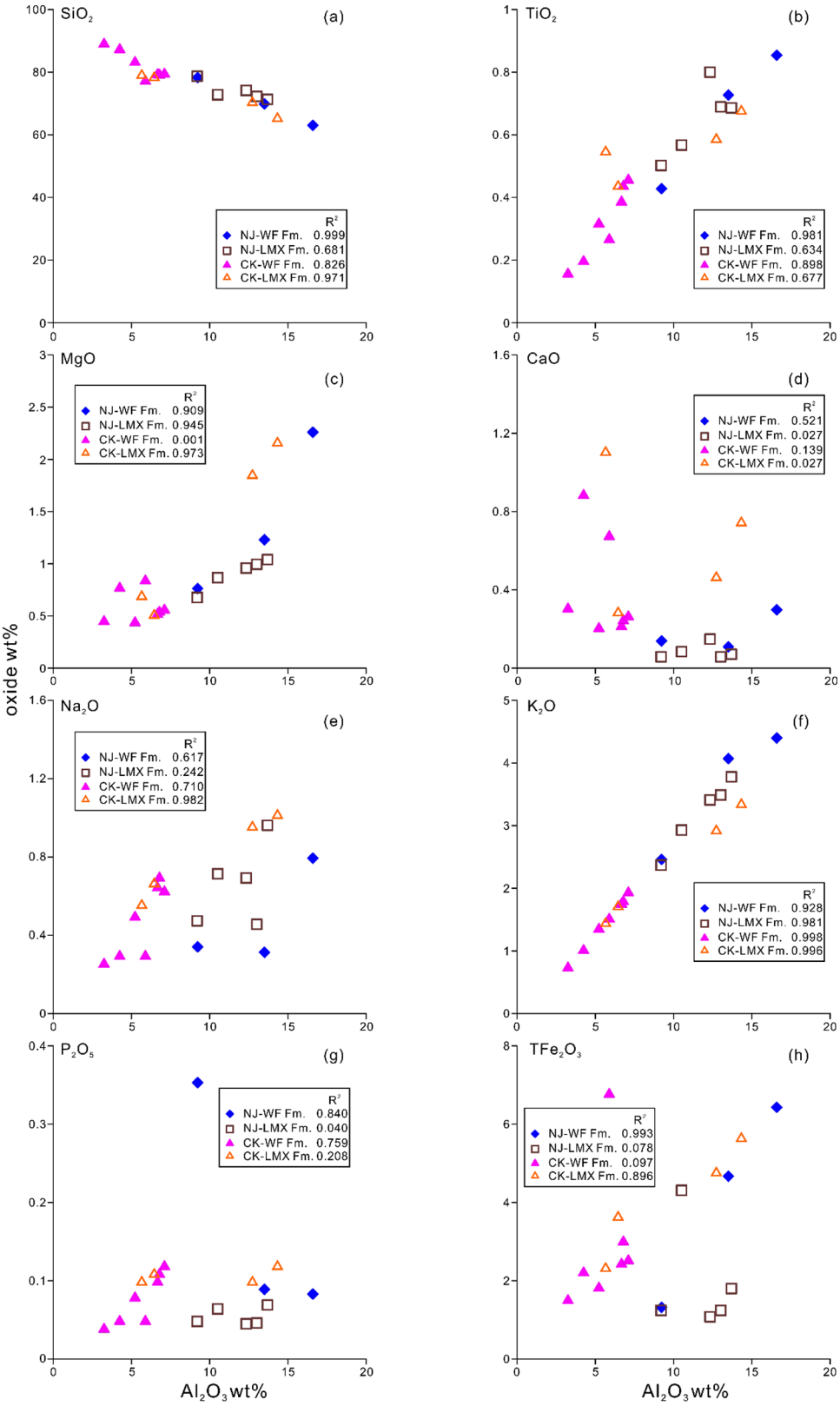

Figure 3. Plots of Al_2O_3 versus the other major element oxide: (a) SiO_2, (b) TiO_2, (c) MgO, (d) CaO, (e) Na_2O, (f) K_2O, (g) P_2O_5, and (h) TFe_2O_3 for the Wufeng and Longmaxi formations in the NJ section in Sichuan Province and the CK section in the Chongqing Municipality, southern China.

digested once again using 0.500 mL (1 + 1) of HNO_3 and 1.50 mL of HF after evaporation, and it was then dried once more (1 + 1). HNO_3 was then added to the sample at a volume of 2.00 mL. After drying the mixture once again, the process was repeated while adding HNO_3. For trace element analysis, the solution was finally diluted with 1.00% HNO_3 to 50.0 mL. The details of the analytical procedures have been described by Guo et al. and Li et al.[29,30] In general, the analytical accuracy of the

https://doi.org/10.1021/acsomega.3c00277
ACS Omega 2023, 8, 13078−13096

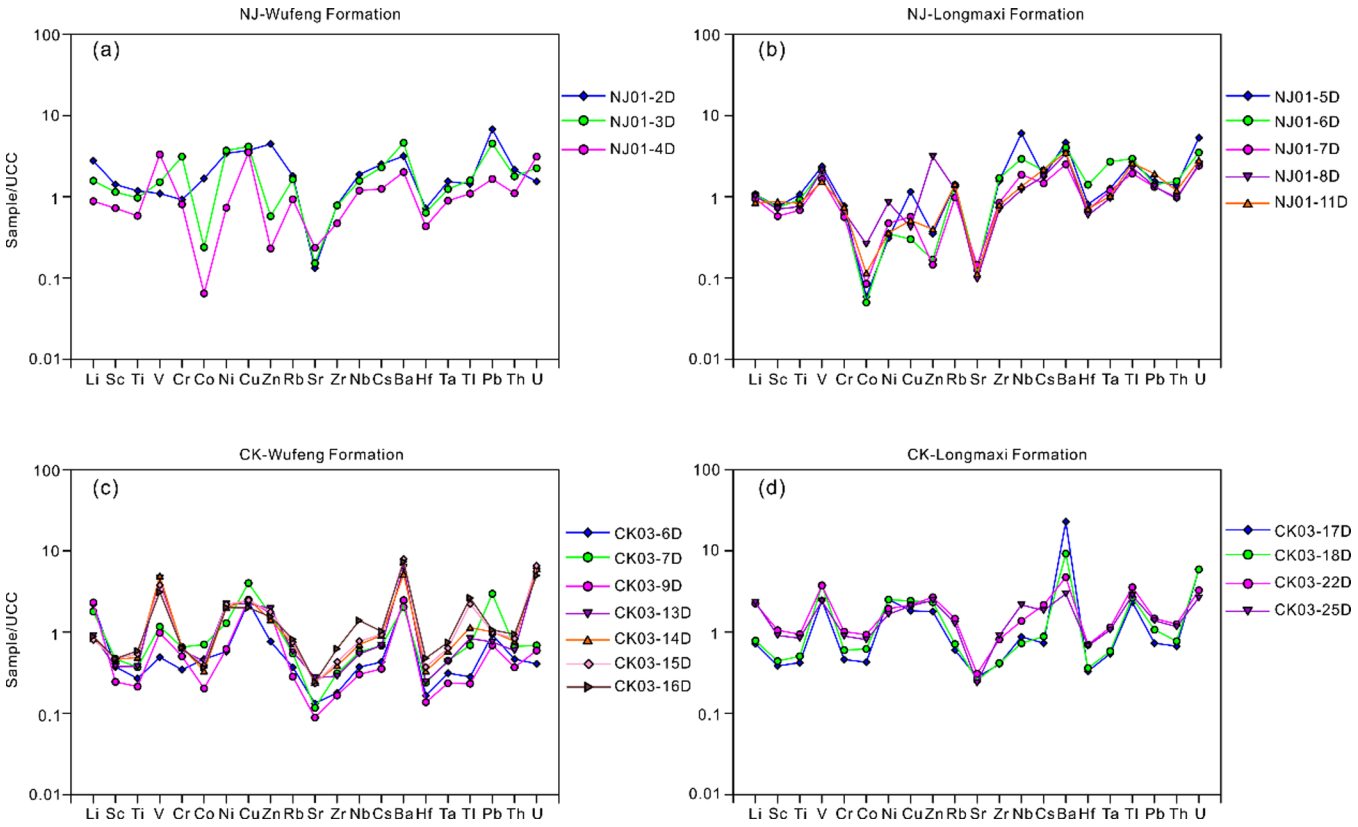

Figure 4. Trace element enrichment factors correlative to average shale or upper continental crust for the (a) Wufeng Formation and (b) Longmaxi Formation in the NJ section in Sichuan Province and the (c) Wufeng Formation and (d) Longmaxi Formation in the CK section in the Chongqing Municipality, southern China.

trace element concentrations exceeded 5%. Further details have been reported by Guo et al. and Li et al.[29,30] In order to protect against the analytical interference of the Eu abnormalities resulting from Ba during inductively coupled plasma source mass spectrometry testing, Dulski's correction method was used[31]

$$\frac{Eu}{Eu^*} = (3 \times Eu_N)/(2 \times Sm_N + Tb_N) \quad (1)$$

$$\frac{Ce}{Ce^*} = Ce_N/(La_N \times Pr_N)^{1/2} \quad (2)$$

$$\frac{Y}{Y^*} = Y_N/(Dy_N \times Ho_N)^{1/2} \quad (3)$$

$$\frac{Pr}{Pr^*} = Pr_N/(Ce_N \times Nd_N)^{1/2} \quad (4)$$

where N indicates that the concentration has been normalized against Post-Archean Australian Shale (PAAS).[32]

The total organic carbon (TOC) was gauged using a LECO CS-200 analyzer after the samples were handled with hydrochloric acid to dislodge the carbonates at the experimental center of Exploration & Development Research Institute, PetroChina Southwest Oil & Gas field Company, Chengdu, Sichuan Province.[25]

4. RESULTS

4.1. Major Elements. Table 1 shows the concentrations of the major elements. The SiO_2 contents of the WF in the NJ section range from 63.02 wt % in sample NJ01-2D to 78.29 wt % in sample NJ01-4D (with an average value of 70.39 wt %), with relatively low average SiO_2 contents in these samples from this formation. For the LMX in the NJ section, the SiO_2 contents range from 71.32 wt % in sample NJ01-11D to 78.7 wt % in sample NJ01-7D (with an average value of 73.84 wt %). The SiO_2 contents of the WF in the CK section range from 77.58 wt % in sample CK03-7D to 89.43 wt % in sample CK03-9D (with an average value of 82.48 wt %), with relatively high average SiO_2 contents in all of the samples from this formation. For the LMX in the CK section, the SiO_2 contents range from 65.64 wt % in sample CK03-22D to 79.42 wt % in sample CK03-17D (with an average value of 73.63 wt %). However, the Al_2O_3 contents are different from the SiO_2 contents. The Al_2O_3 contents of the WF in the NJ section range from 9.23 wt % in sample NJ01-4D to 16.59 wt % in sample NJ01-2D (with an average value of 13.11 wt %), with relatively high average Al_2O_3 contents in all of the samples from this formation. For the LMX in the NJ section, the Al_2O_3 contents range from 9.2 wt % in sample NJ01-7D to 13.69 wt % in sample NJ01-11D (with an average value of 11.75 wt %). The Al_2O_3 contents of the WF in the CK section range from 3.25 wt % in sample CK03-9D to 7.11 wt % in sample CK03-16D (with an average value of 5.6 wt %), with relatively low average Al_2O_3 contents in these samples from this formation. For the LMX in the CK section, the Al_2O_3 contents range from 5.66 wt % in sample CK03-17D to 14.33 wt % in sample CK03-22D (with an average value of 9.79 wt %). The correlations between SiO_2 and $Al2O_3$ in the samples derived from these formations are exhibited to be negative (Figure 3a).

The abundances of TiO_2 (<0.9 wt %), Na_2O (<1.1 wt %), and K_2O (<4.5 wt %) are significantly lower than those of SiO_2 and

https://doi.org/10.1021/acsomega.3c00277
ACS Omega 2023, 8, 13078−13096

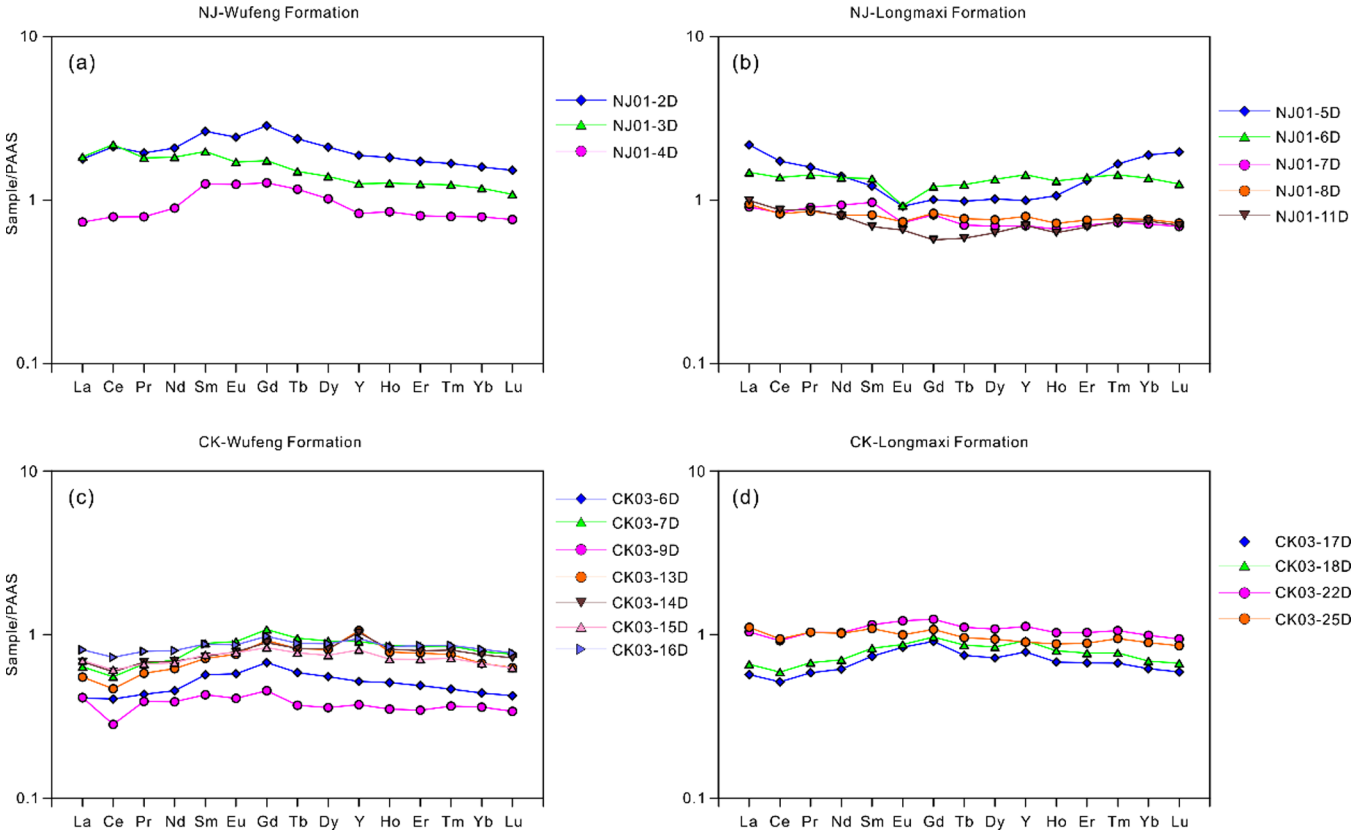

Figure 5. PAAS-normalized REE patterns for the (a) Wufeng Formation and (b) Longmaxi Formation in the NJ section in Sichuan Province and the (c) Wufeng Formation and (d) Longmaxi Formation in the CK section in the Chongqing Municipality, southern China.

Al_2O_3 and exhibit apparent positive correlations with Al_2O_3 (Figure 3b,e,f). The MgO (<2.3 wt %) contents of most of the formations exhibit an apparent positive correlation with Al_2O_3, except for the WF in the CK section (Figure 3c). The CaO content of the WF in the NJ section is positively correlated with the Al_2O_3 content (Figure 3d). However, most of the samples, except for CK03-17D, have extremely low CaO contents (<1.0 wt %), which are not correlated with the Al_2O_3 content (Figure 3d). The P_2O_5 contents are considerably low (<0.36 wt %), and there is a negative correlation between the Al_2O_3 and P_2O_5 contents in the NJ section of the WF (Figure 3g). However, the P_2O_5 contents of the WF in the CK section are positively correlated with the Al_2O_3 content (Figure 3g), and those of the LMX in all of the sections do not exhibit an obvious correlation with the Al_2O_3 content (Figure 3g).

The total iron (TFe_2O_3) content has a wide range (1.08−6.8 wt %). The total iron contents of the WF in the NJ section and the LMX in the CK section are positively correlated with the Al_2O_3 content (Figure 3h). However, the total iron contents of the LMX in the NJ section and the WF in the CK section are not correlated with the Al_2O_3 content (Figure 3h).

4.2. Trace Elements. The analytical results are presented in Table 2. Figure 4 shows the enrichment factors, which are found by dividing the elemental concentration by the average shale (PAAS) or upper continental crust. This is the method used by McLennan.[32] In the NJ section, the different lithofacies have similar amounts of trace elements, with significant increases in Pb > Ba > Cu > V > U > Cs > Nb > Li > Th > Tl > Ta for the shale and mudstone of the WF (Figure 4a) and Nb > U > Ba > Tl > V > Cs > Pb > Th > Ta > Cu > Li for the carbonaceous shale and carbonaceous mudstone of the LMX (Figure 4b). The different lithofacies in the CK section exhibit similar trace element abundances and have large enrichments in Ba > U > V > Cu > Tl > Li > Ni > Zn for the siliceous shale of the WF (Figure 4c) and Ba > U > V > Tl > Ni > Zn > Cu > Li for the siliceous shale and carbonaceous shale of the LMX (Figure 4d).

4.3. Rare Earth Elements. The NJ section samples exhibit total REE contents ranging from 153.6 to 377.9 ppm. The average total REE content gradually exhibits a declining trend from the WF (296.8 ppm) to the LMX (207.9 ppm) (Table 3). The CK section samples exhibit total REE contents ranging from 64.1 to 183.8 ppm. The average total REE content gradually exhibits a rising trend from the WF (107.4 ppm) to the LMX (148.5 ppm) (Table 3). There are obvious differences between the two sections. The specific reasons for this are analyzed in detail in Section 5. Based on the characteristics of the different formations in the different sections, four groups can be made from the PAAS-normalized REE values (Figure 5). Most of the samples from the WF in the NJ section only slightly deviate from the average REE patterns (La_N/Y_{bN}: 0.93−1.55, with an average of 1.20), with weak positive Ce anomalies ($Ce/Ce^*_{avg.}$ = 1.12 ± 0.08, n = 3) and weak negative Eu anomalies ($Eu/Eu^*_{avg.}$ = 0.97 ± 0.06, n = 3), excepting sample NJ01-4D (Eu/Eu* = 1.02) (Figure 5a). The majority of the LMX samples in the NJ section also exhibit slight deviations based on the average REE patterns (La_N/Y_{bN}: 1.09−1.34), with weak negative Ce anomalies ($Ce/Ce^*_{avg.}$ = 0.93 ± 0.02, n = 5) as well as significant negative Eu anomalies ($Eu/Eu^*_{avg.}$ = 0.85 ± 0.15, n = 5), excepting sample NJ01-11D (Eu/Eu* = 1.0) (Figure 5b). Neither the WF in the CK section (Group C) nor the LMX in the CK section (Group D) exhibits flat REE patterns (Group C La_N/Y_{bN}: 0.81−1.15; Group D La_N/Y_{bN}: 0.92−1.24), with $Ce/Ce^*_{avg.}$ = 0.86 ± 0.16

https://doi.org/10.1021/acsomega.3c00277
ACS Omega 2023, 8, 13078−13096

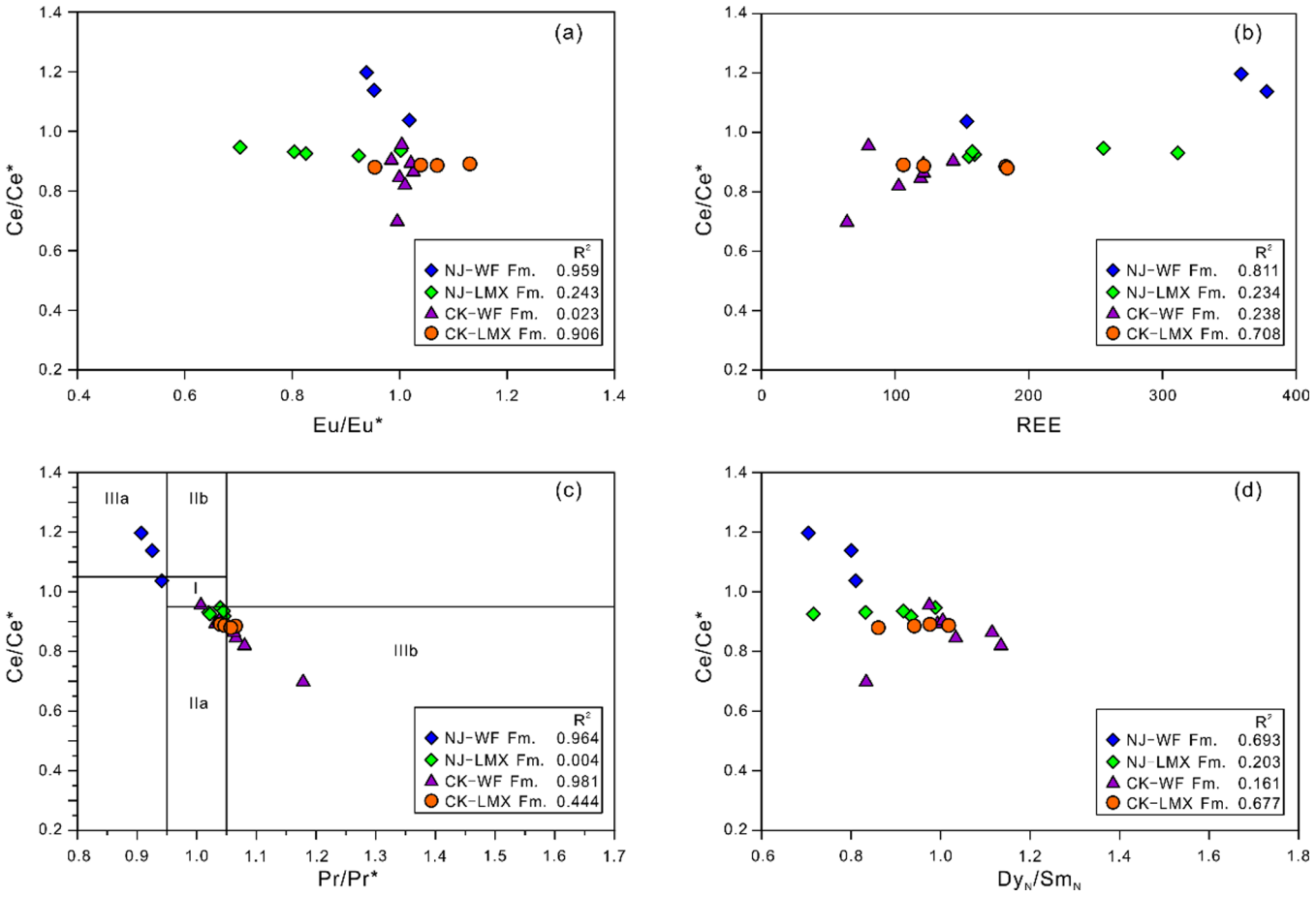

Figure 6. Plots of Ce anomalies versus (a) Eu anomalies, (b) total REE, (c) Pr anomalies, and (d) Dy_N/Sm_N ratios figured out from the PAAS-normalized REE abundances of the organic matter in the sedimentary rocks from the NJ section in Sichuan Province and the CK section in the Chongqing Municipality, southern China.

($n = 7$) and $Eu/Eu^*_{avg.} = 1.01 \pm 0.03$ ($n = 7$) for the WF in the CK section (Group C) and $Ce/Ce^*_{avg.} = 0.89 \pm 0.01$ ($n = 4$) as well as $Eu/Eu^*_{avg.} = 1.05 \pm 0.10$ ($n = 4$) for the LMX in the CK section (Group D) (Figure 5c,d). However, a few samples from the CK section have weak negative Eu anomalies.

5. DISCUSSION

5.1. Distributions of REEs and Cerium Anomalies. The REE distribution pattern of the source area remains almost unchanged during the sedimentary diagenetic processes.[33] The combined effects of seawater adsorption, terrigenous particle composition, and metalliferous particle composition may be seen in the REE concentrations of sedimentary rocks.[34−36] The REEs in the ocean are mainly from rivers.[30,37−39] Terrigenous materials and water masses seldom show light REEs (LREE) fractionation relative to heavy REEs (HREEs),[40,41] but the REE pattern of seawater often shows a significant negative Ce anomaly, weak negative Eu anomaly, and HREE enrichment.[42] In addition, another important feature of seawater is its positive Y anomaly.[43−45] Therefore, the REE pattern is a significant indicator for distinguishing whether sedimentary rocks are dominated by authigenic or detrital components.

In this study, the REE patterns of the shales and mudstones from the NJ-WF Fm. (the WF in the NJ section) commonly exhibit weak positive Ce anomalies and weak negative Y anomalies (average = 0.93) (Figures 5a and 6). The shales and mudstones from the lower NJ-LMX Fm. (the LMX in the NJ section) (NJ01-5D to NJ01-7D) exhibit smooth REE patterns with weak negative Ce anomalies and no Y anomalies (average = 1.02) (Figures 5b and 6). However, the shales from the upper NJ-LMX Fm. (NJ01-8D to NJ01-11D) have weak negative Ce anomalies and weak positive Y anomalies (average = 1.09). The shales and mudstones of the NJ-WF Fm. may have been affected by a variety of factors (e.g., upwelling or hydrothermal activity). The REE patterns of the shales and mudstones of the lower NJ-LMX Fm. indicate that these rocks are typical detrital shales and mudstones, whereas the shales and mudstones of the upper NJ-LMX Fm. have been affected by seawater. The majority of the shale samples from the CK-WF Fm. (the WF in the CK section) and the CK-LMX Fm. (the LMX in the CK section) show flat REE patterns with weak negative Ce anomalies and positive Y anomalies (CK03-13D to CK03-22D, average = 1.16) (Figure 5c,d), which indicates that these shales have been influenced by seawater. The remaining samples were gathered from the lower portion of the CK-WF Fm. and the upper portion of the CK-LMX FM., which are featured by flat REE patterns with weak negative Ce and no Y anomalies (average = 1.01) (Figure 5c,d), indicating that these shales are typical detrital shales. The Y/Ho ratios of the upper part of the CK-WF Fm. and the lower part of the CK-LMX Fm. (samples CK03-13D to CK03-22D, average Y/Ho ratio = 32.21) are distinctly higher than those of the other samples from the CK section (average Y/Ho ratio = 28.38). This indicates that for samples from the upper portion of the CK-WF Fm. and the lower portion of the CK-LMX Fm., the effect of

https://doi.org/10.1021/acsomega.3c00277
ACS Omega 2023, 8, 13078−13096

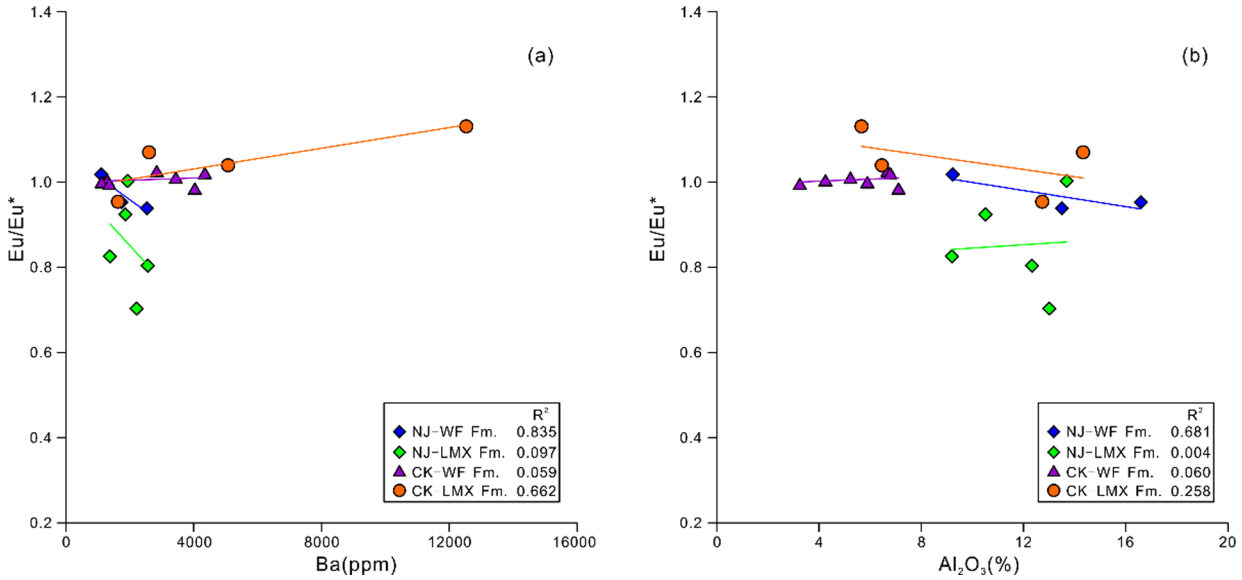

Figure 7. Plots of (a) Eu/Eu* versus Al_2O_3 and (b) Eu/Eu* versus Ba for the NJ section in Sichuan Province and the CK section in the Chongqing Municipality, southern China.

seawater was more significant than the detrital inputs. The comparison of the upper NJ-LMX Fm. and lower NJ-LMX Fm. samples also revealed that they have similar characteristics.

The negative Ce anomaly of seawater is connected to the oxidation of Ce(III) to stationary Ce(IV) and may be used to show fine-grained sediment depositional environments throughout the ocean basin due to continental and spreading ridge impacts and to trace the redox conditions if the samples have not been affected by post-depositional diagenetic REE exchange.[35,37,42,46−49] In this research, the Ce anomalies of the NJ-WF Fm. and CK-LMX Fm. samples interrelate well with the Dy_N/Sm_N ratio (Figure 7d), showing that MREE arching has had an effect on the Ce anomalies. However, the Ce anomalies of the NJ-LMX Fm. and CK-WF Fm. samples have not been influenced by MREE arching. The connection between the Ce anomalies and the total REE contents implies that in the NJ-CK Fm. and CK-LMX Fm. (positive correlation), progressive REE scavenging after deposition was strong.[39] Additionally, Pr/Pr* values of 0.95−1.05 demonstrate that positive La anomalies are causing prominent negative Ce anomalies (Figure 7c).[39] Several samples plot within the genuine Ce anomaly (Figure 7c), but the negative Ce anomalies of several of the samples from the NJ-LMX Fm. (all five samples), CK-WF Fm. (three samples), and CK-LMX Fm. (two samples) are amplified by the enrichment of La. In this research, most samples do not exhibit significant positive Y and La anomalies.

Generally, sediments from anoxic basins and shelves exhibit weak negative to moderate positive Ce anomalies, but moderate to strong negative Ce anomalies indicate well-oxygenated environments.[30,37,42,47] Based on this research, the small negative Ce anomalies may indicate the occurrence of a redox-stratified ocean environment within the Late Ordovician to Early Silurian transition in southern China. We found that the samples from the lower NJ-LMX Fm. (NJ01-5D to NJ01-7D), the lower part of the CK-WF Fm. (CK03-6D to CK03-9D), and the upper CK-LMX Fm. (CK03-25D) have been highly affected by detrital input as was previously discussed. Therefore, we solely discuss the Ce anomalies of the NJ-WF Fm. shales and mudstones, the upper NJ-LMX Fm. shales, the upper part of the CK-WF Fm. shales, and the lower part of the CK-LMX Fm. shales (CK03-13D to CK03-22D), which reflect the original seawater redox conditions.

The NJ-WF Fm. shale and mudstone samples exhibit weak positive Ce anomalies (1.04−1.20), indicating anoxic seawater redox conditions (Figure 6). The upper NJ-LMX Fm. shale samples (NJ01-8D and NJ01-11D) exhibit weak negative Ce anomalies (0.92−0.94), indicating a change in the seawater redox conditions to less anoxic (Figure 6). The upper part CK-WF Fm. shale samples and the lower part of the CK-LMX Fm. shales exhibit weak negative Ce anomalies (0.83−0.91), indicating progressively less anoxic seawater redox conditions (Figure 8). This weak change in the Ce anomalies is compatible with reports of earlier researches regarding the seawater circumstances within the Late Ordovician−Early Silurian transition.

5.2. Europium Anomalies and Hydrothermal Events.

Positive Eu anomalies are highly prevalent in marine hydrothermal sediments and are usually seen in strongly reducing hydrothermal liquids that promote the reduction of Eu^{3+} to Eu^{2+}.[36,44,50−52] None of the samples analyzed in this research have extremely high Ba contents, and there is no momentous positive linear relationship between Ba and Eu/Eu*, except for the CK-LMX Fm. samples (the correlation index is positive, 0.662) (Figure 9a). While detrital feldspar may contribute to positive Eu anomalies,[36] the lack of a momentous positive linear relationship between Al_2O_3 and Eu/Eu* (Figure 9b) for these samples rules out this hypothesis.

Previous researches on the Eu anomalies of Late Ordovician−Early Silurian rocks in Hubei Province and Guizhou Province have offered a number of proofs of hydrothermal input. In conjunction with findings from petrology and stable isotope analyses, the marl with black shale in the Guanyinqiao Member of the Wufeng Fm. in Guizhou Province (Tongzi) demonstrates positive Eu anomalies and variable Y anomalies, exhibiting the effect of hydrothermal liquid.[26,53] In this area, the siliceous shale and carbonaceous shale of the lower NJ-LMX Fm., the lower part of the CK-WF Fm., and the upper part of the CK-LMX Fm. typically have a flat REE pattern devoid of positive Eu anomalies (Figure 5b−d), demonstrating that the lower NJ-LMX Fm., the lower part of the CK-WF Fm., and the upper part of the CK-

https://doi.org/10.1021/acsomega.3c00277
ACS Omega 2023, 8, 13078−13096

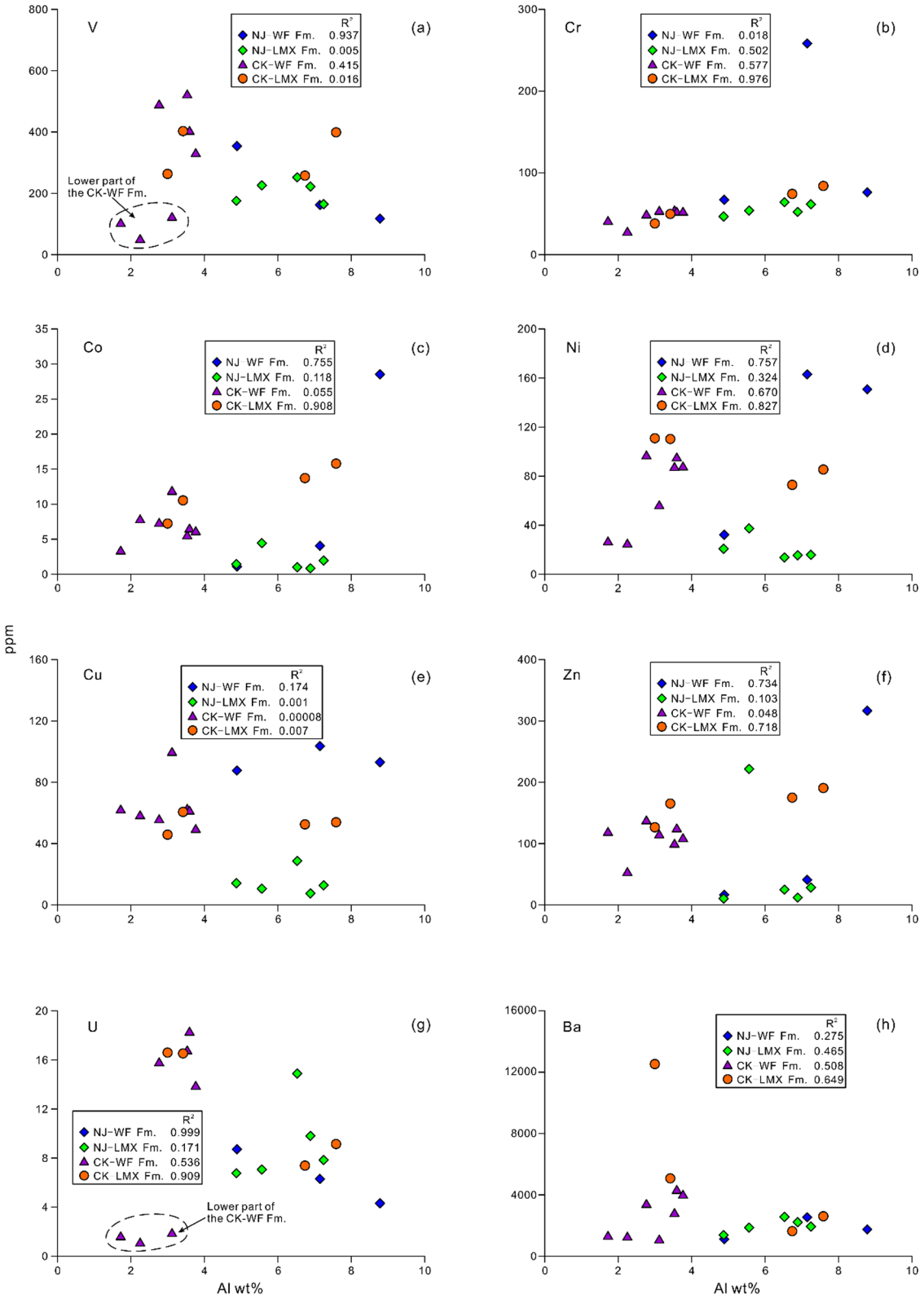

Figure 8. Plots of the major element Al versus trace elements (a) V, (b) Cr, (c) Co, (d) Ni, (e) Cu, (f) Zn, (g) U, and (h) Ba for the Wufeng (WF) and Longmaxi (LMX) formations in the NJ section in Sichuan Province and the CK section in the Chongqing Municipality, southern China.

LMX Fm. were influenced by detrital input. In comparison, the siliceous shale samples (CK03-17D) from the lower part of the CK-LMX Fm. exhibit slight positive Eu anomalies (1.13), weak negative Ce anomalies (0.89), and positive Y anomalies (1.12), demonstrating the combined hydrothermal and seawater characteristics (Figure 5d). However, the majority of the shale samples from the upper part of the CK-WF Fm. and the lower part of the CK-LMX Fm. do not exhibit clear Eu anomalies (average = 1.03). As was previously mentioned, the samples were found to be highly affected by seawater or upwelling

https://doi.org/10.1021/acsomega.3c00277
ACS Omega 2023, 8, 13078−13096

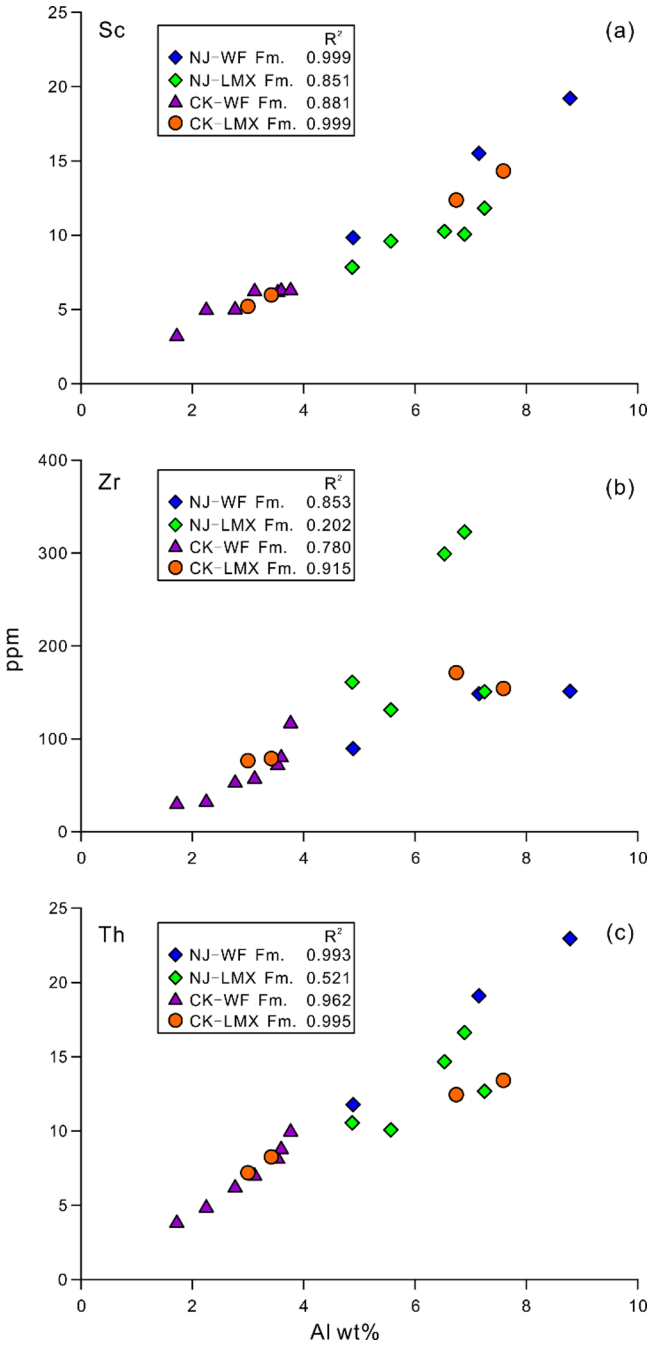

Figure 9. Plots of Al versus (a) Sc, (b) Zr, and (c) Th for the sedimentary rocks in the NJ section in Sichuan Province and the CK section in the Chongqing Municipality, southern China.

because of their flat REE patterns and weak to moderate positive Y anomalies (1.06−1.33, average = 1.16) and because organic detritus derived from seawater and upwelling generally has negative Eu anomalies. Therefore, a plausible interpretation is that the presence of organic detritus in these shale samples likely attenuated the impact of hydrothermal inputs. The NJ-WF Fm. shale and mudstone samples do not exhibit clear Eu anomalies (average = 0.97) and Y anomalies (average = 0.93). These samples might not have been affected by hydrothermal activity, but they were influenced by seawater and upwelling. The hydrothermal activity was not widely distributed within the Late Ordovician−Early Silurian transition, and it might have only been a local event in the Upper Yangtze Platform.

5.3. Trace Element Geochemistry. Both detrital and authigenic components influence the trace element contents of most sediments, but only the contents of the authigenic components alter in return to redox changes in the water column.[54] The trace element contents are often standardized to the Al content to adjust for fluctuating dilution by organic matter and authigenic material in order to correct the authigenic enrichment of a given element.[55] However, when the Al comes from other Al-rich or Al-poor sources, enrichment might be overstated or understated.[56] To overcome this problem, a typical approach is that the Al is plotted against Sc, Th, or Zr, which are likewise composed mostly of detrital, to establish whether it originates from a similar siliciclastic source.[30] If a significant positive correlation is discovered, it is possible to deduce that the Al was originated from a familiar detrital flux.[30] In this research, the samples from the shale and mudstone succession in the NJ and CK sections show a high degree of relationships between Al and Sc, Zr, and Th, indicating that the Al originated from familiar terrigenous sources (Figure 10a−c).

Paleoredox proxies for seawater may be utilized with trace elements like U, V, Co, and Cr.[55,57] However, the correlations between U, V, Co, and Cr and Al for these samples produce inconsistent outcomes (Figure 11). First, the U and V contents of the NJ-WF Fm. samples are not positively relevant to the Al content (Figure 11a,g), demonstrating that the enrichments of U and V were not affected by detrital sources. In contrast, the enrichment of Co in the NJ-WF Fm. exhibits an apparent positive correlation with the Al content (Figure 11c), implying that the concentration of Co was predominantly from the siliciclastic portion of the sediments, which restricts its use as a trustworthy redox proxy. Second, the U and V concentrations of the NJ-LMX Fm. are weakly relevant to the Al content (Figure 11a,g), demonstrating that the enrichments of U and V were highly affected by the redox circumstances but not detrital sources. Conversely, the enrichment of Cr in the NJ-LMX Fm. exhibits an evidently positive relationship with the Al content (Figure 11b). Third, the U and V concentrations of the CK-LMX Fm. are not positively relevant to the Al concentration (Figure 11a,g). However, the enrichments of Cr and Co in the CK-LMX Fm. exhibit evidently positive correlations with the Al concentration (Figure 11b,c). Finally, the U and V concentrations of the CK-WF Fm. exhibit moderate positive correlations with the Al concentration (Figure 11a,g), but we know that the samples from the lower part of the CK-WF Fm. (CK03-06D to CK03-09D) were affected by detrital sources. Therefore, we analyzed the lower and upper a part of CK-WF Fm. separately. We found that the U and V contents of the lower and upper parts of the CK-WF Fm. do not exhibit obvious positive correlations with the Al content (Figure 11a,g). Therefore, in the following sections, apart from the relational ratios of Th/U and V/Sc, the enrichments of U and V are used to research the paleoredox circumstances of the Late Ordovician and Early Silurian shallow sea.

Uranium is mostly found in the soluble form of uranyl carbonate complexes $[UO_2(CO_3)4-3]$ in oxic to suboxic seawater, but under specific reducing circumstances, it can be reduced to U(IV) and precipitate into the sediments as crystalline uraninite (UO_2) or its metastable predecessors.[30,58] Because of bacterial sulfate reduction is in charge of at least a portion of the change from U(VI) to U(IV), the U enrichment under non-sulfidic anoxic circumstances is frequently strongly correlated with the TOC concentration.[59] In this research, the U/Al ratios ($\times 10^{-4}$) of NJ section exhibit slight variations,

https://doi.org/10.1021/acsomega.3c00277
ACS Omega 2023, 8, 13078−13096

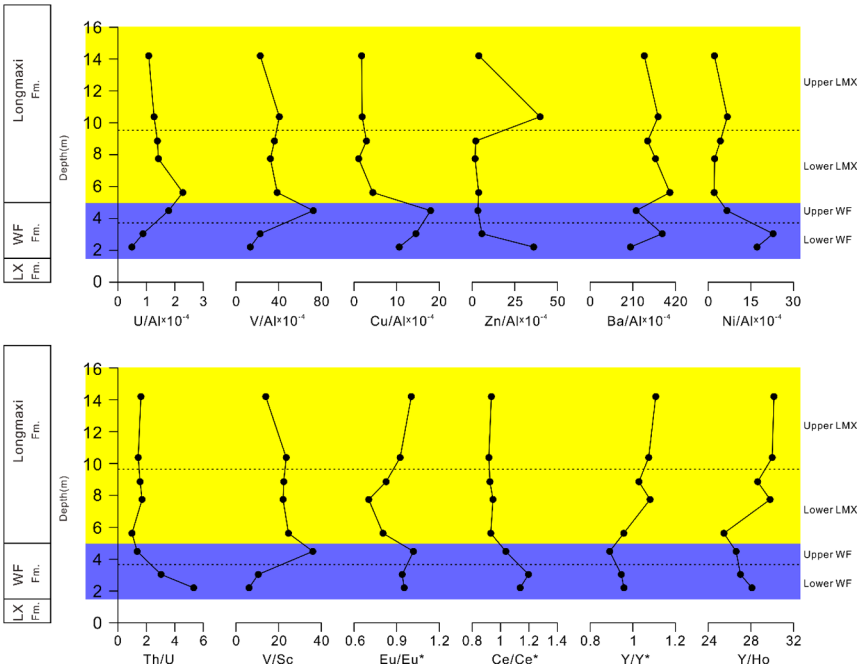

Figure 10. Stratigraphic distributions of the Al-normalized trace element consistences and chosen ratios for the sedimentary rocks in the NJ section in Sichuan Province, southern China. The yellow area denotes the Longmaxi (LMX) Formation, and the blue area denotes the Wufeng (WF) Formation.

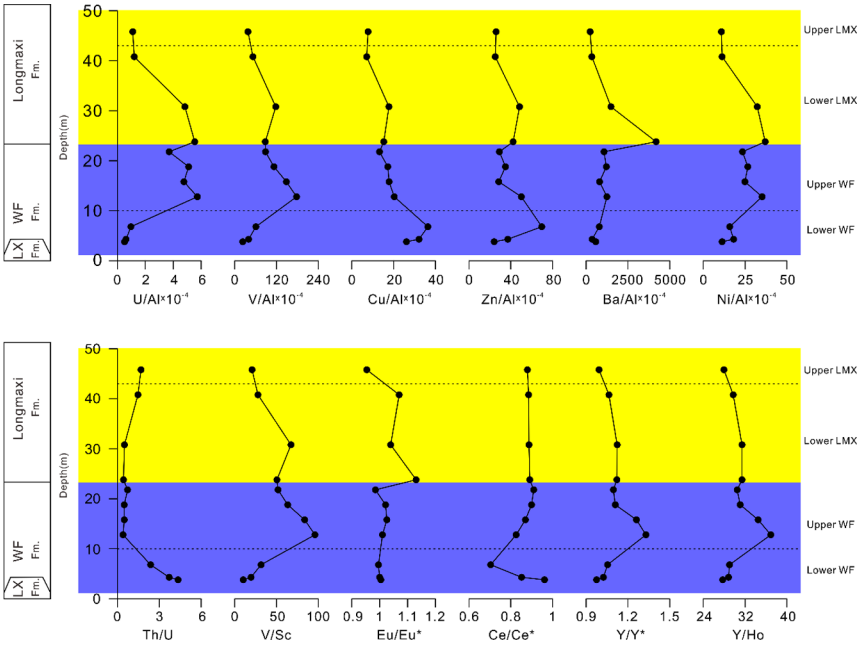

Figure 11. Stratigraphic distributions of the Al-normalized trace element consistences and picked ratios for the sedimentary rocks in the CK section in the Chongqing Municipality, southern China. The yellow area denotes the Longmaxi Formation, and the blue area denotes the Wufeng (WF) Formation.

within the range of 0.491−2.28, from the NJ-WF Fm. siliceous shale to the NJ-LMX Fm. carbonaceous shale (Figure 6). However, the U/Al ratios of the CK section show significant differences, ranging between 0.508 and 5.73, from the CK-WF Fm. siliceous shale to the CK-LMX Fm. carbonaceous shale (Figure 8). All of the samples show strong U enrichment compared to the U/Al ratio of PAAS (0.310).[33] However, compared to Black Sea euxinic sediments (U/Al ratio of 3.30),[55] the upper CK-WF Fm. and the lower CK-LMX Fm. (CK03-13D to CK03-18D) exhibit comparatively high U enrichments, but the vast majority of the sediments of the NJ-WF Fm., NJ-LMX Fm., lower CK-WF Fm., and upper CK-LMX Fm. exhibit variable U depletion. This demonstrates that the upper CK-WF Fm. and the lower CK-LMX Fm. were deposited in a euxinic environment likeness that of the Black Sea, while the overlaying lower CK-WF Fm. siliceous shales and the underlying upper CK-LMX Fm. carbonaceous shales were deposited in a less-reducing setting. Furthermore, the NJ-WF Fm. and NJ-LMX Fm. shales and mudstones were also deposited in a less-reducing setting. However, with the exception of the sample from the NJ-

https://doi.org/10.1021/acsomega.3c00277
ACS Omega 2023, 8, 13078−13096

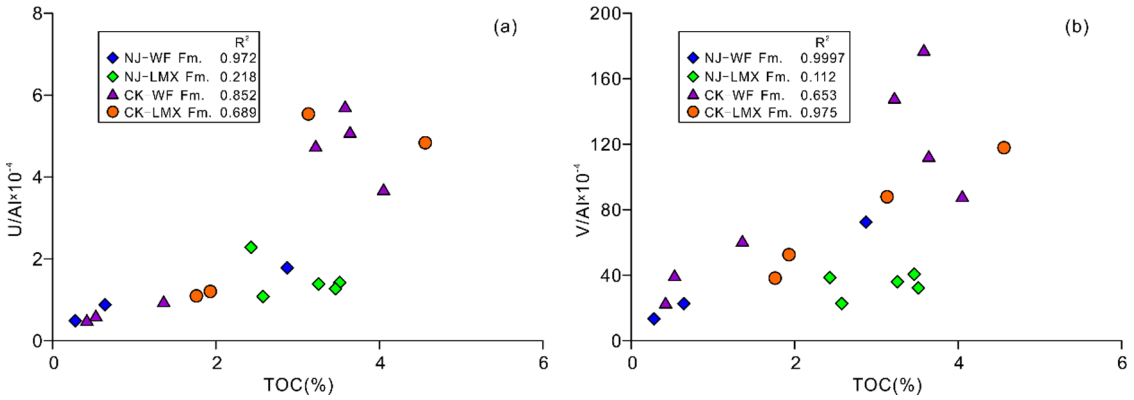

Figure 12. Relationships between TOC and (a) U/Al and (b) V/Al for the samples from the NJ section in Sichuan Province and the CK section in the Chongqing Municipality, southern China.

LMX Fm., the U/Al ratios of the shales and mudstones of both formations are closely associated with the TOC contents. (Figure 12a), which indicates that the redox circumstances were usually anoxic but were not sulphide.[59,60] Since correlations between trace element and TOC contents are more vaild for determining the redox circumstances,[54] the depositional environments of the NJ-WF Fm., CK-WF Fm., and CK-LMX Fm. were possibly anoxic instead of euxinic (sulfidic). Wignall (1996) indicated that anoxic environments result in Th/U ratios between 0 and 2 in shales.[62] Furthermore, earlier researches have shown that Th/U = 2 is a proper demarcation line threshold between oxic and anoxic bottom-water environments.[26,61] In this research, the Th/U ratios of the distinct formations demonstrate redox circumstances consistent with those determined based on the U/Al ratios (Figures 6 and 8). The Th/U ratios of the samples from the lower NJ-WF Fm. (NJ01-2D to NJ01-3D) are greater than 2 (3.03−5.32), indicating oxic conditions. The upper NJ-WF Fm. (only one sample, NJ01-4D) and the NJ-LMX Fm. have low Th/U ratios, having an average value below 1.50, indicating that the upper NJ-WF Fm. and the NJ-LMX Fm. were deposited in a less-reducing setting. The Th/U ratios of the lower CK-WF Fm. are greater than 2 (2.38−4.34), indicating oxic conditions, whereas the Th/U ratios of the upper CK-WF Fm. and lower CK-LMX Fm. are very low, with an average value of less than 0.50, indicating anoxic conditions. The Th/U ratios of the upper CK-LMX Fm. are higher (avg. Th/U = 1.58), indicating less reducing conditions than those of the lower part of the formation. However, it is essential to note that the U enrichment and high Th/U ratios of the lower NJ-WF Fm. shales and mudstones imply that the rocks were deposited under oxic environments, which contradicts the abovementioned conclusion that the Ce anomalies demonstrate deposition under anoxic environments. Nevertheless, the TOC value is low in this part of the formation, and the enrichment of Ce may have been affected by MREE arching.[39] Therefore, the Ce anomaly cannot be utilized as a sign of the redox circumstances of the lower NJ-WF Fm. shales and mudstones.

Under non-sulfidic anoxic environments, the abundance of V generally correlates strongly with the TOC concentration since humic and fulvic acids speed up the reduction of V(V) to V(IV).[30] Conversely, V(IV) is reduced to V(III) in sulfidic environments as well as independent of organic reactions.[30] Therefore, under such conditions, there is no apparent association between V abundance and TOC concentration.[30,63] In this research, the V/Al ratios ($\times 10^{-4}$) of all samples from the NJ-WF Fm. and the NJ-LMX Fm. are within the range of 13.38−72.49 (Figure 6) and are higher than that of PAAS (15.0).[32,33] The V/Al ratios of these samples from the CK-WF Fm. and the CK-LMX Fm. are within the range of 23.31−177.62 (Figure 8) and thus are typically higher than that of PAAS. In contrast to the Black Sea marine setting (V/Al = 28.8),[30,55] most of the samples from the upper NJ-WF Fm., NJ-LMX Fm., CK-WF Fm., and CK-LMX Fm. exhibit significant V enrichment (V/Al ratios = 22.74−177.62), whereas the samples from the lower NJ-WF Fm. exhibit lower depleted values (13.38−22.65). These results seemingly indicate that the upper NJ-WF Fm., NJ-LMX Fm., CK-WF Fm., and CK-LMX Fm. were deposited under sulfidic environments. Nevertheless, the intense relationship between the V enrichment and TOC concentration (Figure 12b) indicates that the upper NJ-WF Fm., CK-WF Fm., and CK-LMX Fm. were under non-sulfidic anoxic conditions, which is more trustworthy.[30] However, the NJ-LMX Fm. exhibits a weak relationship between the V enrichment and TOC concentration (Figure 12b), which may indicate that the NJ-LMX Fm. was deposited in a less reducing environment. Moreover, the V/Sc ratio may be utilized to evaluate redox conditions.[26,30,61] In this study, significant enrichment of V over Sc has occurred in most of the samples from the upper NJ-WF Fm., NJ-LMX Fm., upper CK-WF Fm., and lower CK-LMX Fm., which also have Th/U ratios that are smaller than 2 (Figures 6 and 8), demonstrating that the samples were deposited in anoxic bottom water.

Hydrothermal inputs are a significant source of trace elements as well.[30,54] Previous studies in Hubei Province and Guizhou Province have discovered that the slight enrichments of trace elements in the WF and LMX, especially in the upper WF and the lower LMX, are the consequence of both hydrothermal inputs and seawater.[26,53] Even though the Al-normalized trace elements do not exhibit linear correlations with the Eu anomalies, except for the NJ-WF Fm., U, V, Cu, and Ba are usually enriched in the shales and mudstones of the NJ-LMX Fm., while U, V, Cu, Ni, Zn, and Ba are enriched in the shales of the CK section, particularly the upper CK-WF Fm. and the lower CK-LMX Fm., compared to the other samples (Figures 8 and 13).[30] As was previously mentioned, the REE results demonstrate that the lower CK-LMX Fm. shales have been affected by hydrothermal inputs, while the other formations have been dominated by detritus or seawater affects. This difference in conclusions based on the REEs and trace elements may reflect the different sensitivities of the various indicators to hydrothermal effects. However, the relative consistency between the trace element enrichments and hydrothermal activity

https://doi.org/10.1021/acsomega.3c00277
ACS Omega 2023, 8, 13078−13096

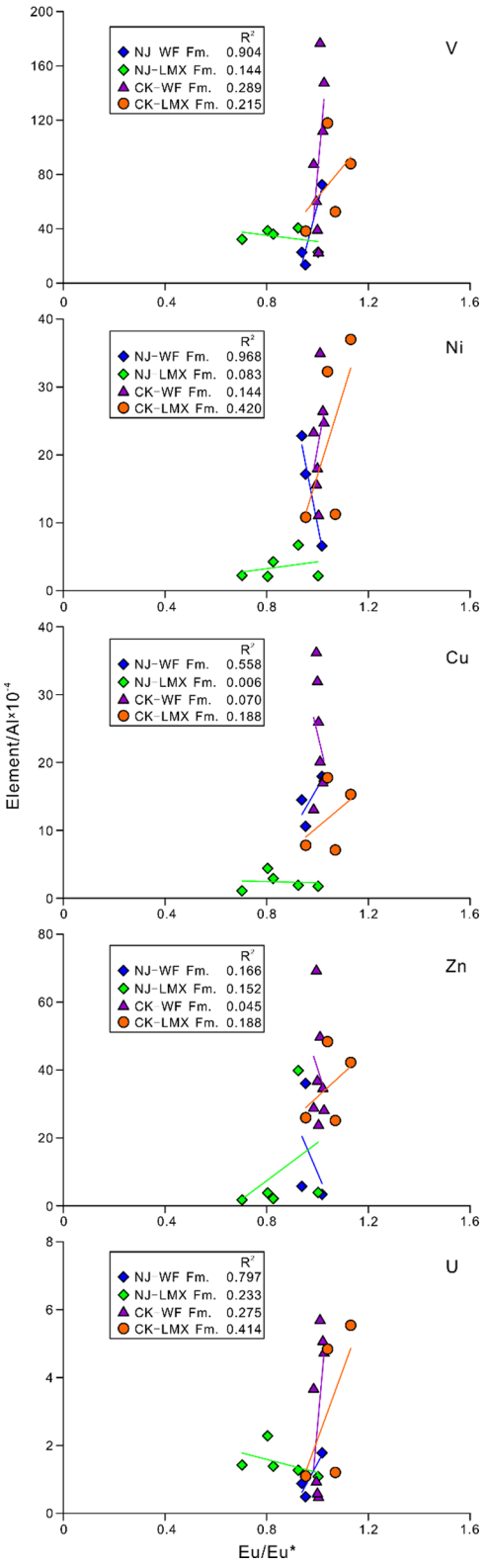

Figure 13. Plots of Eu/Eu* versus Al-normalized trace elements for the Wufeng (WF) and Longmaxi (LMX) formations in the NJ section in Sichuan Province and the CK section in the Chongqing Municipality, southern China.

indicates that the strength of hydrothermal inputs did not directly dominate the contents of trace elements, but they might have enhanced the enrichment of trace elements to a certain extent.

A lot of researches have tried to estimate if metamorphism can influence the way elements are distributed in metasedimentary rocks.[30,64] However, it is difficult to study the local movement of elements caused by metamorphism because the local element variations caused by sedimentary processes are large.[34] In this research, the impacts of metamorphism on element flowability seem to be tiny in relation to the impacts of sedimentary procedures.[30] Prior researches have concentrated on the impacts of burial diagenesis and increasing benthic O_2 levels on the remobilization of redox-sensitive elements in contemporary marine sediments.[30,62,65,66] However, there is little proof of the translocation of redox-sensitive elements under continuously anoxic conditions.[30,59] Further geochemical studies with a higher resolution (cm scale) will be required to assess if restricted diagenetic redistribution of some trace elements has arisen.[26,30,67]

According to the abovementioned research, we can infer that most of the samples from the NJ and CK sections have contemporaneous U and V enrichments compared to PAAS, but only the samples from the upper CK-WF Fm. and the lower CK-LMX Fm. demonstrate contemporaneous U and V enrichments relative to Black Sea sediments. Furthermore, most of the samples from the NJ-WF Fm. and the NJ-LMX Fm. also exhibit V enrichment compared to Black Sea sediments. Therefore, taking into consideration the existence of Ce anomalies in the NJ-WF Fm. and NJ-LMX Fm. samples, we consider that the redox conditions of the NJ section altered from oxic in the lower NJ-WF Fm. to lightly anoxic or dysoxic in the upper NJ-WF Fm. shale, and then, the redox conditions gradually transitioned to anoxic in the NJ-LMX FM. shales and mudstones. Based on the same evidence, we consider that the redox conditions of the CK section altered from oxic in the lower CK-WF FM. to strongly anoxic in the upper CK-WF Fm. and the lower CK-LMX Fm. shales, and then, they gradually transitioned to slightly anoxic in the upper CK-LMX Fm. shales.

5.4. Ocean Environment Changes and Organic Matter Enrichment. A biological mass extinction event occurred in the Late Ordovician.[62,68,69] This extinction event was accompanied by a series of geological events, such as Gondwana glaciers, sea-level fall, volcano eruptions, and the widespread deposition of black shale.[1,6,70−75] Both marine conditions and hydrothermal events have played crucial roles in the formation of the siliceous shales and carbonaceous shales. From the systematic TOC data, we determined that the abundance of organic matter was tightly correlated with the geochemical varieties. As opposed to earlier researches that concentrated on western Hubei and northern Guizhou, this study area is located in northern Sichuan and northeastern Chongqing, which is much closer to the northern margin of the Upper Yangtze Platform, where the effects of hydrothermal venting incidents occurred later and weakened. In the Late Katian, the Middle Katian shallow shelf or carbonate platform was submerged by a transgressive incident. In the Middle Katian, a carbonate platform was developed inside the Yangtze platform. Nonetheless, the sea level stayed at a comparatively low level with significant hydrodynamic energy and no input from hydrothermal incidents as demonstrated by the REE patterns of the lower NJ-WF Fm. and the lower CK-WF Fm. mudstone and siliceous shale. The combination of oxic seawater conditions and large current or wave energy counts against organic matter preservation. Therefore, the TOC concentrations of the lower NJ-WF Fm. and the lower CK-WF Fm. are quite low. In the Late Katian, the Cathaysian Plate compressed the Yangtze Platform from the southeast to the

https://doi.org/10.1021/acsomega.3c00277
ACS Omega 2023, 8, 13078−13096

northwest. Because of the effects of the extrusion of the Cathaysian Plate, a depression formed in the Chengkou area. Despite this moment, the sea level remained relatively shallow in the Nanjiang area. In the Hirnantian, Gondwana glaciation events led to a global sea-level drop, which is indicated by the change in the lithology of the top of the NJ-WF Fm. to gray graywacke. However, due to the effects of the extrusion of the Cathaysian Plate, the seawater continued to deepen in the Chengkou area. Meanwhile, a short part of hydrothermal motion along the fault of the northeastern transition zone slightly impacted the composition of the basal CK-LMX siliceous shale, which is demonstrated by the positive Eu anomalies. Therefore, the circumstances of the upper NJ-WF Fm. and the upper CK-WF Fm. changed to slightly anoxic and strongly anoxic, respectively. The TOC concentrations of the upper CK-WF Fm. are higher than those of the upper NJ-WF Fm. With the ablation of the Hirnantian glacier, the maximum flooding surface was attained by the relative sea level and the Early Silurian shallow sea became quite layered and anoxic. Under the anoxic circumstances of the bottom water, indicated by the trace element proxies, the organic matter from the high plankton production in the photic zone was effectively stored on the seafloor.[30] Therefore, the TOC concentrations of the NJ-LMX Fm. and the lower CK-LMX Fm. are relatively high (2.43−3.51 wt % and 3.13−4.56 wt %, respectively). In conjunction with the anoxic circumstances, the Hirnantian hydrothermal activity episodes slightly accelerated the enrichment of trace elements. As the sea level gradually dropped, the bottom water's reducing conditions weakened, and the organic matter that precipitated from the photic zone was oxidized under the greater amount of oxygen level on the seafloor.[1,14,30] Therefore, the TOC contents of the upper CK-LMX Fm. shales decreased significantly to 1.76−1.93 wt %. Although the change in the productivity in the photic zone also might have affected the organic matter enrichment, the high degree of correlation between the redox circumstances and the TOC enrichment indicates that the redox circumstances played a significant part in the accumulation of organic matter.

6. CONCLUSIONS

To the best of our knowledge, a comprehensive chemostratigraphic study of the Late Ordovician and Early Silurian succession in the northern margin of the Upper Yangtze Platform is presented for the first time in this study. The REE patterns with weak positive Ce anomalies and weak negative Y anomalies of the NJ-WF Fm. demonstrate that the REE concentrations of the fine-grain sedimentary rocks were influenced by oxic seawater conditions or upwelling. The weak negative Ce anomalies and weak positive Y anomalies in the REE patterns of the upper NJ-LMX Fm. carbonaceous shales, the upper CK-WF Fm., and the lower CK-LMX Fm. siliceous shales are indicative of the influence of seawater. Nevertheless, the positive Eu and Y anomalies of the REE patterns of the samples from the base of the CK-LMX Fm. demonstrate that the REEs in the siliceous shale were influenced by hydrothermal fluids. The lack of positive Eu and Y anomalies in the flat REE patterns of the lower NJ-LMX Fm., the lower CK-WF Fm., and the upper CK-LMX Fm. indicates that the REEs in the fine-grain sedimentary rocks were dominated by detrital inputs instead of seawater or hydrothermal input. The sudden change in the Th/U and V/Sc ratios in the upper NJ-WF Fm. and the upper CK-WF Fm. suggests a considerable decline in the oxygen level in the seawater in the Late Katian. The Al-normalized U and Al-normalized V enrichments, and the related Th/U and V/Sc ratios, demonstrate that the redox circumstances of the bottom water were different in different areas during the Ordovician−Silurian transition. In the NJ area, the redox circumstances of the bottom water during the Ordovician−Silurian transition changed from oxic in the Late Katian to slightly anoxic in the Hirnantian and then progressively became anoxic in the Early Rhuddanian. However, in the CK area, the redox circumstances of the bottom water during the Ordovician−Silurian transition suddenly changed from oxic in the Late Katian to strongly anoxic in the Hirnantian and continued to become more anoxic until the Rhuddanian. The significant correlations between the TOC concentration and U and V enrichments indicate that the upper NJ-WF Fm., NJ-LMX Fm., upper CK-WF Fm., and lower CK-LMX Fm. mudstones and shales were deposited under non-sulfidic anoxic circumstances. Apart from the anoxic circumstances, episodic hydrothermal inputs in the Hirnantian further promoted the enrichment of trace elements in the CK area.

AUTHOR INFORMATION

Corresponding Author

Xuan Liu − *College of Mining, Liaoning Technical University, Fuxin 123000, China;* orcid.org/0000-0003-1185-9446; Email: 1772166746@qq.com

Authors

Xiang Fu − *College of Mining, Liaoning Technical University, Fuxin 123000, China*

Shuzhen Xiong − *College of Environmental Science and Engineering, Liaoning Technical University, Fuxin 123000, China*

Xu Li − *China Coal Technology & Engineering Group Shenyang Research Institute, Fushun 113122, China*

Qixuan Wu − *College of Mining, Liaoning Technical University, Fuxin 123000, China*

Bin Xiao − *College of Mining, Liaoning Technical University, Fuxin 123000, China*

Complete contact information is available at: https://pubs.acs.org/10.1021/acsomega.3c00277

Notes

The authors declare no competing financial interest.

ACKNOWLEDGMENTS

This study was funded by the National Science and Technology Major Project of China (Grant No. 2017ZX05005003-007) and the Project of the Liaoning Provincial Natural Science Fund (Grant No. 2022-BS-328).We also value the assistance offered by the Liaoning Technological University Discipline Innovation Team (Grant Nos. LNTU20TD-14 and LNTU20TD-30).We appreciate the language support LetPub (www.letpub.com) provided throughout the development of this paper.

REFERENCES

(1) Li, Y. F.; Zhang, T. W.; Ellis, G. S.; Shao, D. Y. Depositional environment and organic matter accumulation of Upper Ordovician−Lower Silurian marine shale in the Upper Yangtze Platform, South China. *Palaeogeogr., Palaeoclimatol., Palaeoecol.* **2017**, *466*, 252−264.

(2) Melchin, M. J.; Mitchell, C. E.; Holmden, C.; Storch, P. Environmental changes in the Late Ordovician-early Silurian: Review and new insights from black shales and nitrogen isotopes. *Geol. Soc. Am. Bull.* **2013**, *125*, 1635−1670.

(3) Su, W.; Li, Z.; Ettensohn, F. R.; Johnson, M. E.; Huff, W. D.; Wang, W.; Zhao, H. Tectonic and eustatic control on the distribution of black-shale source beds in the Wufeng and Longmaxi formations (Ordovician-Silurian), South China. *J. Front. Earth Sci. China* **2007**, *1*, 470−481.
(4) Yan, D.; Chen, D.; Wang, Q.; Wang, J. Predominance of stratified anoxic Yangtze Sea interrupted by short-term oxygenation during the Ordo-Silurian transition. *Chem. Geol.* **2012**, *291*, 69−78.
(5) Zhang, Z.; Xu, T.; Zhao, B.; Badal, J. Systematic variations in seismic velocity and reflection in the crust of Cathaysia: New constraints on intraplate orogeny in the South China continent. *Gondwana Res.* **2013**, *24*, 902−917.
(6) Brenchley, P. J.; Carden, G. A.; Hints, L.; Kaljo, D.; Marshall, J. D.; Martma, T.; Nõlvak, J. High-resolution stable isotope stratigraphy of Upper Ordovician sequences: Constraints on the timing of bioevents and environmental changes associated with mass. *Geol. Soc. Am. Bull.* **2003**, *115*, 89−104.
(7) Jones, D. S.; Fike, D. A. Dynamic sulfur and carbon cycling through the end-Ordovician extinction revealed by paired sulfate-pyrite δ34S. *Earth Planet. Sci. Lett.* **2013**, *363*, 144−155.
(8) Saltzman, M. R.; Young, S. A. Long-lived glaciation in the Late Ordovician? Isotopic and sequence-stratigraphic evidence from western Laurentia. *Geology* **2005**, *33*, 109−112.
(9) Armstrong, H. A.; Abbott, G. D.; Turner, B. R.; Makhlouf, I. M.; Muhammad, A. B.; Pedentchouk, N.; Peters, H. Black shale deposition in an Upper Ordovician-Silurian permanently stratified, peri-glacial basin, southern Jordan. *Palaeogeogr., Palaeoclimatol., Palaeoecol.* **2009**, *273*, 368−377.
(10) Xiao, B.; Liu, S. G.; Ran, B.; Li, Z. W. Geochemistry and sedimentology of the Upper Ordovician−lower Silurian black shale in the northern margin of the Upper Yangtze Platform, South China: Implications for depositional controls on organic-matter accumulation. *Aust. J. Earth Sci.* **2020**, *67*, 129−150.
(11) Lüning, S.; Shahin, Y. M.; Loydell, D.; Al-Rabi, H. T.; Masri, A.; Tarawneh, B.; Kolonic, S. Anatomy of a world-class source rock: Distribution and depositional model of Silurian organic-rich shales in Jordan and implications for hydrocarbon potential. *AAPG Bull.* **2005**, *89*, 1397−1427.
(12) Vecoli, M.; Riboulleau, A.; Versteegh, G. J. M. Palynology, organic geochemistry and carbon isotope analysis of a latest Ordovician through Silurian clastic succession from borehole Tt1, Ghadamis Basin, southern Tunisia, North Africa: Palaeoenvironmental interpretation. *Palaeogeogr., Palaeoclimatol., Palaeoecol.* **2009**, *273*, 378−394.
(13) Chen, X.; Rong, J. Y.; Li, Y.; Boucot, A. J. Facies patterns and geography of the Yangtze region, South China, through the Ordovician and Silurian transition. *Palaeogeogr., Palaeoclimatol., Palaeoecol.* **2004**, *204*, 353−372.
(14) Liu, Y.; Li, C.; Algeo, T. J.; Fan, J.; Peng, P. Global and regional controls on marine redox changes across the Ordovician-Silurian boundary in South China. *Palaeogeogr., Palaeoclimatol., Palaeoecol.* **2016**, *463*, 180−191.
(15) Su, W.; Huff, W. D.; Ettensohn, F. R.; Liu, X.; Zhang, J.; Li, Z. K-bentonite, black-shale and flysch successions at the Ordovician-Silurian transition, South China: Possible sedimentary responses to the accretion of Cathaysia to the Yangtze Block and its implications for the evolution of Gondwana. *Gondwana Res.* **2009**, *15*, 111−130.
(16) Xiao, B.; Xiong, L.; Zhao, Z. H.; Fu, X. Sedimentary tectonic pattern of Wufeng and Longmaxi Formations in the northern margin of Sichuan Basin, South China. *Int. Geol. Rev.* **2022**, *64*, 2166−2185.
(17) Zhou, L. J.; Zhou, X. H.; Fan, C. J.; Bai, G.; Yang, L.; Wang, Y. Q. Modelling of flue gas injection promoted coal seam gas extraction incorporating heat-fluid-solid interactions. *Energy* **2023**, *268*, 126664.
(18) Guo, X. S.; Li, Y. P.; Tenger, B.; Wang, Q.; Yuan, T.; Shen, B. J.; Ma, Z. L.; Wei, F. B. Hydrocarbon generation and storage mechanisms of deep-water shelf shales of Ordovician Wufeng Formation−Silurian Longmaxi Formation in Sichuan Basin, China. *Pet. Explor. Dev.* **2020**, *47*, 204−213.
(19) Xiao, B.; Liu, S. G.; Li, Z. W.; Ran, B.; Ye, Y. H.; Yang, D.; Li, J. X. Geochemical characteristics of marine shale in the Wufeng Formation−Longmaxi Formation in the northern Sichuan Basin, South China and its implications for depositional controls on organic matter. *J. Pet. Sci. Eng.* **2021**, *203*, 108618.
(20) Chen, X.; Fan, J. X.; Zhang, Y. D.; Wang, H. Y.; Chen, Q.; Wang, W. H.; Liang, F.; Guo, W.; Zhao, Q. Subdivision and delineation of the Wufeng and Lungmachi black shales in the subsurface areas of the Yangtze platform. *J. Stratigraph.* **2015**, *39*, 351−358.
(21) Liang, F.; Bai, W. H.; Zou, C. N.; Wang, H. Y.; Wu, J.; Ma, C.; Zhang, Q.; Guo, W.; Sun, S. S.; Zhu, Y. M.; Cui, H. Y.; Liu, D. X. Shale gas enrichment pattern and exploration significance of Well WuXi-2 in northeast Chongqing, NE Sichuan Basin. *Pet. Explor. Dev.* **2016**, *43*, 386−394.
(22) Zhou, Y. X.; Ding, J.; Yu, Q.; Wang, J.; Men, Y. P.; Xiong, G. Q.; Xiong, X. H.; Deng, Q. Sedimentary and organic carbon isotopic characteristics of the Kuanyinchiao Member in northeastern Chongqing and its regional correlation. *Acta Geol. Sin.* **2017**, *91*, 1097−1107.
(23) Xiao, B.; Xiong, L.; Zhao, Z. Y.; Fu, X.; Zhao, Z. H.; Hou, H. H.; Liu, S. G. Late Ordovician-Early Silurian extension of the northern margin of the Upper Yangtze Platform (South China) and its impact on organic matter accumulation. *J. Pet. Sci. Eng.* **2023**, *220*, 111238.
(24) Huang, F.; Chen, H.; Hou, M.; Zhong, Y.; Jie, A. Filling process and evolutionary model of sedimentary sequence of Middle-Upper Yangtze craton in Caledonian(Cambrian-Silurian). *Acta Petrol. Sin.* **2011**, *27*, 2299−2317.
(25) Ran, B.; Liu, S. G.; Jansa, L.; Sun, W.; Yang, D.; Ye, Y. H.; Zhang, C. J. Origin of the Upper Ordovician-lower Silurian cherts of the Yangtze block, South China, and their palaeogeographic significance. *J. Asian Earth Sci.* **2015**, *108*, 1−17.
(26) Yan, D. T.; Chen, D. Z.; Wang, Q. C.; Wang, J. G. Geochemical changes across the Ordovician-Silurian transition on the Yangtze Platform, South China. *Sci. China Ser. D: Earth Sci.* **2009**, *52*, 38−54.
(27) Chen, X.; Melchin, M. J.; Sheets, H. D.; Mitchell, C. E.; Fan, J. X. Patterns and Processes of Latest Ordovician Graptolite Extinction and Recovery Based on Data From South China. *J. Paleontol.* **2005**, *79*, 842−861.
(28) Fan, J. X.; Melchin, M. J.; Chen, X.; Wang, Y.; Zhang, Y. D.; Chen, Q.; Chen, F. Biostratigraphy and geography of the Ordovician-Silurian Lungmachi black shales in South China. *Sci. China: Earth Sci.* **2011**, *54*, 1854−1863.
(29) Guo, Z.; Hertogen, J.; Liu, J.; Pasteels, P.; Boven, A.; Punzalan, L.; Zhang, W. Potassic magmatism in western Sichuan and Yunnan Provinces, SE Tibet, China: Petrological and geochemical constraints on petrogenesis. *J. Petrol.* **2005**, *46*, 33−78.
(30) Li, Y. F.; Fan, T. L.; Zhang, J. C.; Zhang, J. P.; Wei, X. J.; Hu, X. L.; Zeng, W. T.; Fu, W. Geochemical changes in the Early Cambrian interval of the Yangtze Platform, South China: Implications for hydrothermal influences and paleocean redox conditions. *J. Asian Earth Sci.* **2015**, *109*, 100−123.
(31) Dulski, P. Interferences of oxide, hydroxide and chloride analyte species in the determination of rare earth elements in geological samples by inductively coupled plasma-mass spectrometry. *Fresenius' J. Anal. Chem.* **1994**, *350*, 194−203.
(32) McLennan, S. M. Rare earth elements in sedimentary rocks; influence of provenance and sedimentary processes. *Rev. Mineral. Geochem.* **1989**, *21*, 169−200.
(33) Taylor, S. R.; Mclennan, S. M. *The Continental Crust : Its Composition andEvolution : an Examination of the Geochemical Record Preserved in Sedimentary Rocks*; Black-well Scientific Publications: Oxford, 1985; pp. 1−312.
(34) Cullers, R. L. The geochemistry of shales, siltstones and sandstones of Pennsylvanian-Permian age, Colorado, USA: Implications for provenance and metamorphic studies. *Lithos* **2000**, *51*, 181−203.
(35) Murray, R. W.; Buchholtz Ten Brink, M. R.; Gerlach, D. C.; Price Russ, G.; Jones, D. L. Rare earth, major, and trace element composition of Monterey and DSDP chert and associated host sediment: Assessing the influence of chemical fractionation during diagenesis. *Geochim. Cosmochim. Acta* **1992**, *56*, 2657−2671.

https://doi.org/10.1021/acsomega.3c00277
ACS Omega 2023, 8, 13078−13096

(36) Owen, A. W.; Armstrong, H. A.; Floyd, J. D. Rare earth element geochemistry of upper Ordovician cherts from the Southern Uplands of Scotland. *J. Geol. Soc.* **1999**, *156*, 191−204.
(37) Holser, W. T. Evaluation of the application of rare-earth elements to paleoceanography. *Palaeogeogr., Palaeoclimatol., Palaeoecol.* **1997**, *132*, 309−323.
(38) Nothdurft, L. D.; Webb, G. E.; Kamber, B. S. Rare earth element geochemistry of Late Devonian reefal carbonates, Canning Basin, Western Australia: Confirmation of a seawater REE proxy in ancient limestones. *Geochim. Cosmochim. Acta* **2004**, *68*, 263−283.
(39) Shields, G.; Stille, P. Diagenetic constraints on the use of cerium anomalies as palaeoseawater redox proxies: An isotopic and REE study of Cambrian phosphorites. *Chem. Geol.* **2001**, *175*, 29−48.
(40) Condie, K. C. Another look at rare earth elements in shales. *Geochim. Cosmochim. Acta* **1991**, *55*, 2527−2531.
(41) Sholkovitz, E. R. Rare-earth elements in marine sediments and geochemical standards. *Chem. Geol.* **1990**, *88*, 333−347.
(42) Elderfield, H.; Greaves, M. J. The rare earth elements in seawater. *Nature* **1982**, *296*, 214−219.
(43) Bau, M.; Dulski, P. Distribution of yttrium and rare-earth elements in the Penge and Kuruman iron-formations, Transvaal Supergroup, South Africa. *Precambrian Res.* **1996**, *79*, 37−55.
(44) Douville, E.; Bienvenu, P.; Charlou, J. L.; Donval, J. P.; Fouquet, Y.; Appriou, P.; Gamo, T. Yttrium and rare earth elements in fluids from various deep-sea hydrothermal systems. *Geochim. Cosmochim. Acta* **1999**, *63*, 627−643.
(45) Nozaki, Y.; Alibo, D. S. Importance of vertical geochemical processes in controlling the oceanic profiles of dissolved rare earth elements in the northeastern Indian Ocean. *Earth Planet. Sci. Lett.* **2003**, *205*, 155−172.
(46) Sholkovitz, E. R.; Landing, W. M.; Lewis, B. L. Ocean particle chemistry: The fractionation of rare earth elements between suspended particles and seawater. *Geochim. Cosmochim. Acta* **1994**, *58*, 1567−1579.
(47) Wilde, P.; Quinby-Hunt, M. S.; Erdtmann, B. D. The whole-rock cerium anomaly: a potential indicator of eustatic sea-level changes in shales of the anoxic facies. *Sediment. Geol.* **1996**, *101*, 43−53.
(48) Felitsyn, S.; Morad, S. REE patterns in latest neoproterozoic-early Cambrian phosphate concretions and associated organic matter. *Chem. Geol.* **2002**, *187*, 257−265.
(49) German, C. R.; Elderfield, H. Application of the Ce anomaly as a paleoredox indicator: The ground rules. *Paleoceanography* **1990**, *5*, 823−833.
(50) Michard, A.; Albarede, F. The rare earth element content of some hydrothermal fluids. *Chem. Geol.* **1986**, *55*, 51−60.
(51) Olivarez, A. M.; Owen, R. M. The europium anomaly of seawater: implications for fluvial versus hydrothermal REE inputs to the oceans. *Chem. Geol.* **1991**, *92*, 317−328.
(52) Ruhlin, D. E.; Owen, R. M. The rare earth element geochemistry of hydrothermal sediments from the East Pacific Rise: Examination of a seawater scavenging mechanism. *Geochim. Cosmochim. Acta* **1986**, *50*, 393−400.
(53) Wang, C. S.; Chen, X. H.; Wang, X. Late Orovician Chemical Anomaly And The Environmrntal Changes Across The Orovician-Silurian Boundary In Yangtze Gorges. *J. Stratigraph.* **2002**, *26*, 272−279.
(54) Tribovillard, N.; Algeo, T. J.; Lyons, T.; Riboulleau, A. Trace metals as paleoredox and paleoproductivity proxies: An update. *Chem. Geol.* **2006**, *232*, 12−32.
(55) Calvert, S.; Pedersen, T. Geochemistry of Recent oxic and anoxic marine sediments: Implications for the geological record. *Mar. Geol.* **1993**, *113*, 67−88.
(56) Kryc, K. A.; Murray, R. W.; Murray, D. W. Al-to-oxide and Ti-to-organic linkages in biogenic sediment: Relationships to paleo-export production and bulk Al/Ti. *Earth Planet. Sci. Lett.* **2003**, *211*, 125−141.
(57) Algeo, T. J.; Lyons, T. W. Mo-total organic carbon covariation in modern anoxic marine environments: Implications for analysis of paleoredox and paleohydrographic conditions. *Paleoceanography* **2006**, *21*, 279−298.
(58) Anderson, R. F.; Fleisher, M. Q.; LeHuray, A. P. Concentration, oxidation state, and particulate flux of uranium in the Black Sea. *Geochim. Cosmochim. Acta* **1989**, *53*, 2215−2224.
(59) Algeo, T. J.; Maynard, J. B. Trace-element behavior and redox facies in core shales of Upper Pennsylvanian Kansas-type cyclothems. *Chem. Geol.* **2004**, *206*, 289−318.
(60) Chen, C.; Mu, C. L.; Zhou, K. K.; Liang, W.; Ge, X. Y.; Wang, X. P.; Zheng, B. S. The geochemical characteristics and factors controlling the organic matter accumulation of the Late Ordovician-Early Silurian black shale in the Upper Yangtze Basin, South China. *Mar. Pet. Geol.* **2016**, *76*, 159−175.
(61) Guo, Q.; Shields, G. A.; Liu, C.; Strauss, H.; Zhu, M.; Pi, D.; Yang, X. Trace element chemostratigraphy of two Ediacaran-Cambrian successions in South China: Implications for organosedimentary metal enrichment and silicification in the Early Cambrian. *Palaeogeogr., Palaeoclimatol., Palaeoecol.* **2007**, *254*, 194−216.
(62) Wignall, P. B.; Twitchett, R. J. Oceanic Anoxia and the End Permian Mass Extinction. *Science* **1996**, *272*, 1155−1158.
(63) Morford, J. L.; Emerson, S. The geochemistry of redox sensitive trace metals in sediments. *Geochim. Cosmochim. Acta* **1999**, *63*, 1735−1750.
(64) Moss, B. E.; Haskin, L. A.; Dymek, R. F. Compositional variations in metamorphosed sediments of the Littleton Formation, New Hampshire, and the Carrabassett Formation, Maine, at sub-hand specimen, outcrop, and regional scales. *Am. J. Sci.* **1996**, *296*, 473−505.
(65) Sawlan, J. J.; Murray, J. W. Trace metal remobilization in the interstitial waters of red clay and hemipelagic marine sediments. *Earth Planet. Sci. Lett.* **1983**, *64*, 213−230.
(66) Thomson, J.; Jarvis, I.; Green, D. R. H.; Green, D. A.; Clayton, T. Mobility and immobility of redox-sensitive elements in deep-sea turbidites during shallow burial. *Geochim. Cosmochim. Acta* **1998**, *62*, 643−656.
(67) Abanda, P. A.; Hannigan, R. E. Effect of diagenesis on trace element partitioning in shales. *Chem. Geol.* **2006**, *230*, 42−59.
(68) Chen, X.; Xiao, C.; Chen, H. Wufenian (Ashgillian) graptolite faunal differentiation and anoxic environment in South China. *Acta Palaeontol. Sin.* **1987**, *26*, 326−344.
(69) Wang, K.; Orth, C. J.; Attrep, M.; Chatterton, B. D. E.; Wang, X.; Li, J. J. The great latest Ordovician extinction on the South China Plate: Chemostratigraphic studies of the Ordovician-Silurian boundary interval on the Yangtze platform. *Palaeogeogr., Palaeoclimatol., Palaeoecol.* **1993**, *104*, 61−79.
(70) Brenchley, P. J.; Marshall, J.; Carden, G.; Robertson, D.; Long, D.; Meidla, T.; Anderson, T. Bathymetric and Isotopic Evidence for a Short-Lived Late Ordovician Glaciation in a Greenhouse Period. *Geology* **1994**, *22*, 295−298.
(71) Davies, J. R.; Waters, R. A.; Molyneux, S. G.; Williams, M.; Zalasiewicz, J. A.; Vandenbroucke, T. R. A. Gauging the impact of glacioeustasy on a mid-latitude early Silurian basin margin, mid Wales, UK. *Earth-Sci. Rev.* **2016**, *156*, 82−107.
(72) Delabroye, A.; Vecoli, M. The end-Ordovician glaciation and the Hirnantian Stage: A global review and questions about Late Ordovician event stratigraphy. *Earth-Sci. Rev.* **2010**, *98*, 269−282.
(73) Fan, J.; Peng, P.; Melchin, M. J. Carbon isotopes and event stratigraphy near the Ordovician-Silurian boundary, Yichang, South China. *Palaeogeogr., Palaeoclimatol., Palaeoecol.* **2009**, *276*, 160−169.
(74) Finnegan, S.; Bergmann, K.; Eiler, J. M.; Jones, D. S.; Fike, D. A.; Eisenman, I.; Fischer, W. W. The magnitude and duration of late Ordovician-early Silurian glaciation. *Science* **2011**, *331*, 903−906.
(75) Yan, D.; Chen, D.; Wang, Q.; Wang, J. Large-scale climatic fluctuations in the latest Ordovician on the Yangtze block, South China. *Geology* **2010**, *38*, 599−602.

https://doi.org/10.1021/acsomega.3c00277
ACS Omega 2023, 8, 13078−13096